ABSTRACT

Title of Document: **QUANTUM MECHANICAL INVESTIGATION ON THE VIBRATIONAL RELAXATION OF HF IN COLLISIONS WITH H ATOMS**

Liang Tao, Doctor of Philosophy, 2007

Directed By: **Professor Millard H. Alexander**
Department of Biochemistry and Chemistry,
Institute for Physical Science and Technology,
and Chemical Physics Program
University of Maryland College Park

We investigate the vibrational relaxation of HF(v=2–5) in collisions with H atoms by means of fully-quantum reactive scattering calculations. Our calculations are based on the global *ab initio* potential energy surface of Stark and Werner which includes, specifically, an accurate description on the reaction barrier and the van der Waals wells in the reactant and product arrangements.

We attribute discrepancies between early fluorescence experiments and quasi-classical trajectory calculations to accuracies in the approximate potential energy surface used, in particular inaccuracies in the predicted barrier heights.

By suitable linear combinations of the definite parity basis functions, we are able to separate the nominally indistinguishable inelastic relaxation pathways:

(1) Inelastic vibrational relaxation unaccompanied by H atom exchange

$$H' + HF(v) \rightarrow H' + HF(v' < v)$$

(2) Inelastic vibrational relaxation accompanied by H atom exchange

$$H' + HF(v) \rightarrow H + H'F(v' < v)$$

In addition, reactive quenching also contributes to the overall vibrational removal of HF

$$H' + HF(v) \rightarrow H_2(v'=0) + F$$

We report state-to-state and overall integral cross sections for each of these channels. The dominant removal process corresponds to vibrational relaxation without H-atom exchange. The magnitude of the vibrational relaxation cross sections are in reasonable overall agreement with the limited experimental data.

We also observe sharp structure in the energy dependence of the HF(v=3) removal cross sections. We use an adiabatic-bender analysis to assign this structure to scattering resonances arising from quasi-bound van der Waals states in the HF–H entrance valley.

QUANTUM MECHANICAL INVESTIGATION ON THE VIBRATIONAL RELAXATION OF HF IN COLLISIONS WITH H ATOMS

By

Liang Tao

Dissertation submitted to the Faculty of the Graduate School of the
University of Maryland, College Park, in partial fulfillment
of the requirements for the degree of
Doctor of Philosophy
2007

Advisory Committee:
Professor Millard H. Alexander, Chair
Professor Amy Mullin
Professor Daniel Kosov
Professor Christopher Jarzynski
Professor Stephen Wallace

Dedication

To that one brave heart

To that 30 lonely nights

To that moment landing in California

…

Table of Contents

List of Tables

List of Figures

Chapter 1: Vibrational Relaxation of HF(v) Molecules by H Atoms in the Hydrogen Fluoride Chemical Laser System

1.1. Introduction

Interest in the vibrational relaxation of HF(v) molecules by H atoms dates back to the efforts to understand and model the HF chemical laser.[1-4] In a chemical laser, energy liberated from an exothermic chemical reaction produces the necessary population inversion. The hydrogen fluoride (H_2+F_2) chemical laser is the most extensively studied of all chemical lasers. The detailed kinetics of the laser is fairly complex. The list of major processes that must be considered to model and understand the (H_2+F_2) chemical laser is shown in Table 1.1. The highly exothermic ($\Delta E \sim -32$ kcal/mol) reaction of atomic hydrogen with molecular fluorine (pumping) can produce significant amounts of HF in high vibrational states.[5]

Vibrationally excited HF can be deactivated by collisions with H_2,[6] F, H, other buffer gasses and by collision with HF itself. As a result, overall collisional deactivation is an involved process involving a combination of vibrational-rotational/translational (V→R, T) energy transfer, vibrational-vibrational (V→V) energy transfer, reactive quenching, or other processes (such as wall collisions).[4] The successful operation of chemical lasers such as the HF laser, requires that the

pumping of excited vibrational levels be rapid with respect to collisional removal and decay by spontaneous emissions.

Table 1.1 Reaction scheme in the (H_2+F_2) chemical laser system

(1) Initiation	$F_2 \rightarrow 2F$
(2) Pumping	$F+H_2 \rightarrow HF(v)+H$ $H+F_2 \rightarrow HF(v)+F$
(3) Vibrational relaxation (vibrational to translational and rotational energy transfer)	$HF(v)+M \rightarrow HF(v-1)+M$ M=H, F, He, H_2, F_2, HF $H_2(v)+M \rightarrow H_2(v-1)+M$
(4) Vibration-vibration energy transfer	$HF(v)+HF(v') \rightarrow HF(v+1)+HF(v'-1)$ $HF(v)+H_2(v') \rightarrow HF(v+1)+H_2(v'-1)$ $H_2(1)+H_2(1) \rightarrow H_2(2)+H_2(0)$
(5) Reactive quenching	$HF(v)+H \rightarrow H+F+H \rightarrow H_2+F$
(6) Chain branching	$HF(v \geq 4)+F_2 \rightarrow 2F+HF(0)$
(7) Stimulated emission	$HF(v)+h\nu \rightarrow HF(v-1)+2h\nu$ $HF(v, j)+h\nu' \rightarrow HF(v, j-1 \text{ or } j-2)+2h\nu'$
(8) Rotational relaxation	$HF(v, j)+M \rightarrow HF(v, j')+M$

Early classical trajectory calculations[7,8] indicated that H atoms are the dominant deactivators in hydrogen halide laser systems. Thus, in the presence of excess atomic hydrogen, reactions of H atoms with vibrationally excited states of HF can be an important mechanism by which laser emission is terminated and the laser system is brought to chemical equilibrium. This occurs by a combination of vibration-rotation/translation (V→R, T) processes.[1,9]

The vibrational relaxation of HF(v) molecules by H atoms can proceed by three channels (Fig.1.1) : (1) inelastic vibrational relaxation unaccompanied by H atom exchange

$$H'+HF(v) \rightarrow H'+HF(v'<v) \tag{1.1a}$$

(2) inelastic vibrational relaxation accompanied by H atom exchange

$$H'+HF(v) \rightarrow H+H'F(v'<v) \tag{1.1b}$$

and (3) reactive quenching

$$H'+HF(v) \rightarrow H_2(v'=0)+F \tag{1.1c}$$

As is illustrated schematically in Fig. 2.1, because the $F+H_2 \rightarrow HF+H$ reaction is endoergic by 1.388 eV (32.01 kcal/mol),[10] the last process (1.1c) is possible only for sufficiently high degrees of HF vibrational and/or rotational excitation, or for sufficiently high translational energy.

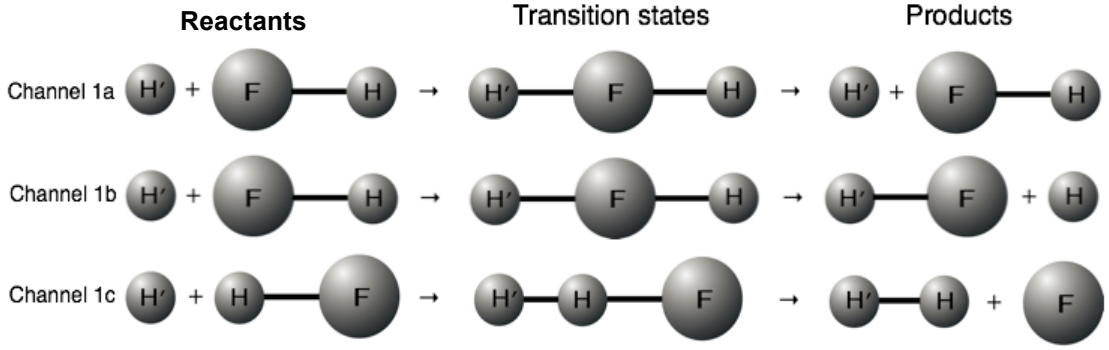

Figure 1.1 Schematic drawing showing three channels of vibrational relaxation of HF(v) in collisions with H atoms

1.2. Experimental study of HF+H vibrational relaxation

Bott and Heidner[11-13] reported an early experimental study of the deactivation of HF in v=3, 2 and 1 by collision with H at temperatures between T=200 and 295K. Vibrationally excited HF was produced by sequential absorption of infrared laser photons from a pulsed, transverse-excitation, atmospheric-pressure HF laser. The hydrogen atoms were created by a microwave discharge in H_2. The absolute concentration of H atoms as a function of time was measured by isothermal calorimetry. The decay of the H atom concentration was assumed to be equal to the decay of the vibrationally excited HF molecules.

The decay times of HF(v=3, 2 and 1) were measured with the microwave discharge on (τ_{on}) and with the discharge off (τ_{off}) at the same flow rates. If pseudo first-order conditions are assumed ([HF] >> [H]) then the overall removal rate constant for HF(v=1, 2, or 3), which is designated *k*, can be determined as follows:

$$\tau_{on}^{-1} - \tau_{off}^{-1} = k[H] \tag{1.2}$$

where [H] is the concentration of H atoms. This removal rate constant *k* represents a sum over removal by the three different channels [Eq. (1.1)]. Unfortunately, the experiment of Bott and Heidner cannot separate out these individual channels.

In the experiments in which the HF(v=3) removal rate was measured, τ_{on} was 5 to 20 times smaller than τ_{off}. In those studies in which the HF(v=2) removal rate was measured, τ_{on} was only slightly shorter than τ_{off} at approximately the same H atom concentrations used for the HF(v=3) experiment. From the data obtained at several temperatures, Bott and Heidner[11-13] concluded that the overall removal rate

constant for HF(v=3) is a factor of 100 faster than that for HF(v=2), while the rate for HF(v=2) removal was found to be only four times faster than the comparable process involving v=1.

1.3. Vibrational relaxation of HF(v=3) by H atoms

1.3.1. Channel (1.1c)

Quasi-classical trajectory (QCT) calculations were carried out by Wilkins and Tompson[8] based on a semiempirical London-Eyring-Polanyi-Sato (LEPS)[14] potential energy surface. In the endothermic abstraction reaction of H with HF, these calculations[7,8] show that vibrational energy will be more effective than translational or rotational energy in bringing about this reaction. This is because the transition state is collinear, so, as shown in Fig. 1.1, vibration leads directly to the bond breaking and forming which are necessary for the reaction to occur. As a corollary, for the collinear approach the QCT calculations suggest that main inelastic (HF+H) energy transfer process involves vibrational energy conversion into translational energy and the minor energy transfer process is for vibrational energy to be converted into rotational energy.

In the experiments of Bott and Heidner,[11-13] the upper limit for the $H' + HF(v) \rightarrow H_2 + F$ abstraction reaction rate constant was estimated to be 3.0×10^{13} cm^3/mol-sec at T=295K. The observed temperature dependence of k(v=3) was fitted by Bott and Heidner to the expression

$$k(\mathrm{v}=3) = 1.7 \times 10^{13} T^{0.179} e^{-760/RT} \quad . \tag{1.3}$$

As mentioned earlier in the introduction, the QCT calculations predicted fast rate constants for the H+HF(v) abstraction with v≥3. The calculated values were fitted to an expression similar to Eq. (1.3), namely

$$k(\mathrm{v}=3) = 10^{13.21} T^{0.010} e^{-835/RT} \tag{1.4}$$

Fig. 1.2 shows the dependence on temperature of the $\mathrm{H'+HF(v=3) \rightarrow H_2+F}$ rate constants predicted by Eqs. (1.3) and (1.4).

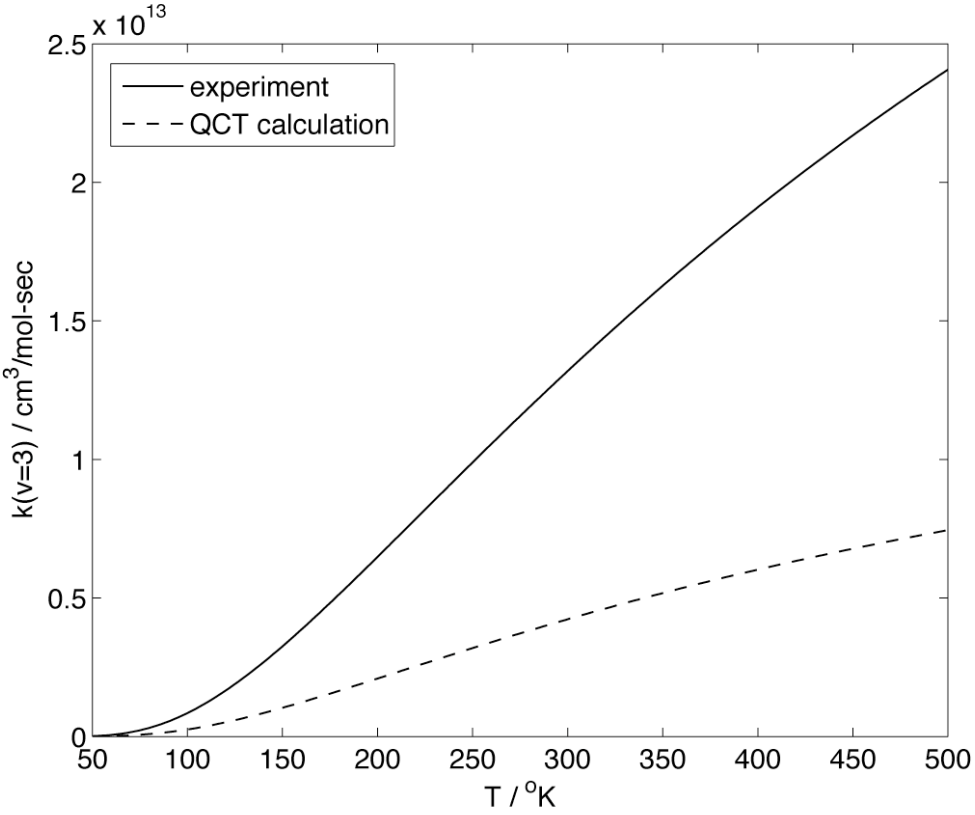

Figure 1.2 Comparison of the temperature dependence of the experimental estimate [Eq. (1.3)] and the QCT prediction [Eq. (1.4)] of the rate constant for the $\mathrm{H'+HF(v=3) \rightarrow H_2+F}$ reaction

1.3.2. Channel (1.1a)+(1.1b)

As already mentioned, the inelastic deactivation of vibrationally excited hydrogen fluoride HF(v) can occur in two different ways: (1.1a) transfer of vibrational energy into translational energy without H-atom exchange, and (1.1b) transfer of vibrational energy into translational energy with H-atom exchange. The first process corresponds to a non-reactive inelastic collision. When the H atom collides with HF(v) molecule, the HF(v) molecule loses or gains vibration energy and ends up in a final vibrational state v′ as HF(v′). The second process corresponds, in reality, to a reactive collision. When the H atom collides with an HF(v) molecule, the incident H atom replaces the H atom from HF(v), and a new HF(v′) molecule is formed in a lower vibrational state.

The QCT calculations of Wilkins and Thompson[8,15] show that the vibrational energy of HF(v) is converted mainly into translational energy in these two processes. The total QCT deactivation rate constants for both processes was fitted as

$$k(v=3) = 10^{13.21} T^{0.010} e^{-646/RT} \tag{1.5}$$

At T=295K, the deactivation rate constant for v=3 was calculated to be 1.7×10^{13} cm^3/mol-sec. It is not clear from the article by Wilkins and Thompson what exactly were the barrier heights in the LEPs surface they used. Bott and Heidner mentioned that Wilkins and Thompson had used values of 1.5, 2.5 and 40 kcal/mole[12] for the exchange reaction (process (1.1b)).

1.3.3. Channel (1.1a)+(1.1b)+(1.1c)

If Bott and Heidner's estimated rate constant $(1.4 \pm 1.5) \times 10^{13}$ cm^3/mol-sec for channel (1.1c) is subtracted from the experimental measurement, then the rate constant to be ascribed to the sum of channels (1.1a) and (1.1b) is $(5 \pm 3) \times 10^{13}$ cm^3/mol-sec. The trajectory calculations on LEPS surface do not predict as fast a rate. The comparison between the experimental measurement and QCT results at T=295K is shown in Table 1.2. We observe that the QCT rate constants for the overall removal process are ~3 times smaller than experiment.

Table 1.2 Relaxation rate constants (cm^3/mol-sec) of HF(v=3) by H atoms at T=295K

	$k_{total}(v=3)$	$k_{channel(1c)}(v=3)$	$k_{channel(1a)+(1b)}(v=3)$	Reference
Experimental measurements	$(6.3 \pm 1.5) \times 10^{13}$	$(1.4 \pm 1.5) \times 10^{13}$	$(5 \pm 3) \times 10^{13}$	12
QCT calculations	2.1×10^{13}	4.1×10^{12}	1.7×10^{13}	8

1.4. Vibrational relaxation of HF(v=2,1) by H atoms

Because the energy of HF(v=2)+H lies below the F+H_2 asymptote, the deactivation of HF(v=2,1) by H atoms can proceed only by the inelastic channels (1.1a) and (1.1b). As shown in Table 1.3, the QCT calculated rates are approximately

10 times faster than the quenching measurement, likely because Wilkins and Thompson were using the LEPS surface which has a low barrier height (1.5kcal/mol or 2.5kcal/mol) for exchange of the fluorine. As the result of the imposition of an artificially low reaction barrier, QCT calculations predicted that inelastic exchange process provides an alternative mechanism for the efficient relaxation of a diatomic molecule, since the rate constant for the deactivation of HF(v=2,1) molecules by H atoms resulting from reactive collisions is nearly 4 times that found for the deactivation of HF(v=2,1) molecules by H atoms resulting from non-reactive collisions. Table 1.3 shows the relaxation rates at T=295K.

Table 1.3 Relaxation rate constants for HF(v=2,1) by H atoms at T=295K

v		$k_{total}(v)$ cm^3/mol-sec	$k_{channel(1a)}(v)$ cm^3/mol-sec	$k_{channel(1b)}(v)$ cm^3/mol-sec	Reference
2	Experimental measurements	$(6.6 \pm 3) \times 10^{11}$			13
	QCT calculations	9.5×10^{12}			8
1	Experimental measurements	$(1.4 \pm 0.4) \times 10^{11}$			13
	QCT calculations	2.6×10^{12}	5.1×10^{11}	2.1×10^{12}	8

1.5. Discrepancies and Questions

The careful *ab initio* study by Stark and Werner (SW)[16] of the FH_2 potential energy surface (PES) predicts a reaction barrier for channel (1.1b) that lies above the v=1 and 2 states of HF. The numerical values of the barriers heights will be presented in Table 2.1**.** If the HF+H translational energy is not enough to surmount such a high barrier, then atom exchange will not contribute. Consequently, we would expect that calculations based on the SW PES will not support the conclusion from previous QCT calculations that the high efficiency of H atoms in relaxing vibrationally excited HF(v=1,2) molecules can be attributed to F atom abstraction from HF(v=1,2) molecules by translationally hot H atoms.

The deactivation rates of HF(v) by H atoms can be expected to increase with v.[3] As mentioned earlier, experiment shows that the rate constant for HF(v=2) removal by H appears to be 4 times faster then the comparable process involving v=1; however, the removal of HF(v=3) by H atoms is faster by a factor 100 than that for HF(v=2). The results of trajectory calculations predict that the rate constants will increase by a factor ~3 from v=1 to v=2 but only ~2–3 from v=2 to v=3. These disagreements might be due to accuracies in the early potential energy surface used, in particular inaccuracies in the predicted barrier heights.

The first goal of our work, presented here, is the use of more modern techniques to investigate HF vibrational relaxation in collisions with H atoms. We

shall base our calculations on the fully *ab initio* PES of Stark and Werner.[16] Furthermore, instead of quasi-classical trajectory calculations, we shall use fully quantum mechanical scattering calculations to determine cross sections and rate constants for collisions of H with HF(v) with v=2–5. In particular, we wish to answer the following questions:

(1) For the collisional deactivation of HF(v=3) by H atoms, classical trajectory calculations on the LEPS surface cannot explain the very fast deactivation rate of HF(v=3) observed from the laser-induced fluorescence experiments. We shall attempt to resolve this discrepancy and also to predict the extent to which the $H'+HF(v=3) \rightarrow H_2+F$ reaction contributes to the overall deactivation.

(2) For relaxation of highly vibrational states of $HF(v \geq 3)$, are multiple-quantum transitions ($\Delta v>1$) more probable than are single-quantum transitions ($\Delta v=1$)? In more detail, what are the product vibrational state distributions for relaxation of each initial vibrational state?

(3) In the classical trajectory calculations, the deactivation of HF(v=2) occurred by both reactive and nonreactive collisions when a potential energy surface with low barriers was used, but solely by non-reactive collisions when the barrier was taken to be 40 kcal/mol. What will quantum mechanical calculations on an accurate *ab initio* potential energy surface show?

(4) The vibrational relaxation of HF(v) by H involves a combination of vibration-rotation/translation (V→R,T) processes. How, specifically, is the

vibrational energy distributed among rotation and translation? How do these distributions vary with initial translational and vibrational energy?

In the course of our investigation we discovered that the presence of quasi-bound states trapped in the weak HF(v=3)–H van der Waals well can enhance the probability of vibrational relaxation. The role of these quasi-bound states, and their connection with calculated peaks in the energy dependence of the calculated cross sections will be explored in Chapter 5 of this dissertation.

Chapter 2: Potential Energy Surface

2.1. Ab initio Stark-Werner potential energy surface (SW-PES)

In 1996, Knowles, Stark and Werner[16,17] presented the first configuration interaction study of the global H–F–H potential energy surface. This SW-PES can be characterized by the following five various stationary points: (a) a linear saddle point (reaction barrier) 41.16 kcal/mol for the symmetric $H'+HF \rightarrow H+H'F$ reaction; (b) a bent barrier of 32.84 kcal/mol high barrier for the $H'+HF \rightarrow H_2+F$ reaction; (c) a linear saddle point of a 33.23 kcal/mol high barrier for $H'+HF \rightarrow H_2+F$ reaction; (d) A C_{2v} symmetry van der Waals well in the $F+H_2$ product valley; (e) A $C_{\infty v}$ symmetry well in both the $H'+HF$ reactant and $H+H'F$ product valleys. The list of these stationary point properties of the SW-PES is given in Table 2.1. The list of barriers to the HF(v=0,1,2,3)+H′→H′F+H reaction is given in Table 2.2. The relative reactant energies, the position of the barriers and wells, and the position of the indicated $F+H_2$ and $H+H'F$ channels have been drawn to scale on the SW-PES in Fig. 2.1.

Table 2.1 Stationary points on the SW-PES for the $H'+HF(v) \rightarrow H+H'F(v'<v)$ and $H'+HF(v) \rightarrow H_2(v')+F$ reactions.

	R_{HF}[a]	r_{HH}[a]	E[b]	E[c]	Angle[d]
H′+HF→H′F+H collinear barrier	2.125	2.125	41.16	1.78	0
H′+HF→F+H_2 bent barrier	2.922	1.457	32.84	1.42	61
H′+HF→F+H_2 colinear barrier	2.950	1.442	33.23	1.44	0
Well depth in F+H_2 arrangement	4.89	1.40	0.37	0.016	90
Well depth in H′+HF arrangement.	4.19	1.74	0.25	0.011	0

a. Distances in bohr, angles in degree.
b. Energies in kcal/mol
c. Energies in eV
d. Bending angles in degree

Table 2.2 Barriers to the HF(v)+H′→H′F+H reaction. [a]

	E_a	
v	eV	kcal/mol
0	1.72	39.66
1	1.23	28.36
2	0.76	17.53
3	0.31	7.15
4	-0.12	-2.79

a. The barrier to HF(v=3)+H′→H_2(v=0)+F is 0.01eV (0.25 kcal/mol)

As shown in Fig. 2.1 and Table 2.2, the bent barrier lies 0.25 kcal/mol (0.01 eV) above the HF(v=3) state. This small barrier will certainly be overcome in reactive quenching process except at very low collision energy. The collinear barrier lies quite high above the HF(v=3) state (0.31 eV) but a little below the HF(v=4) state (0.12 eV). As we can see qualitatively in Table 2.2, inelastic collisions with H atom exchange at collision energies below 0.31eV can proceed only by tunneling.

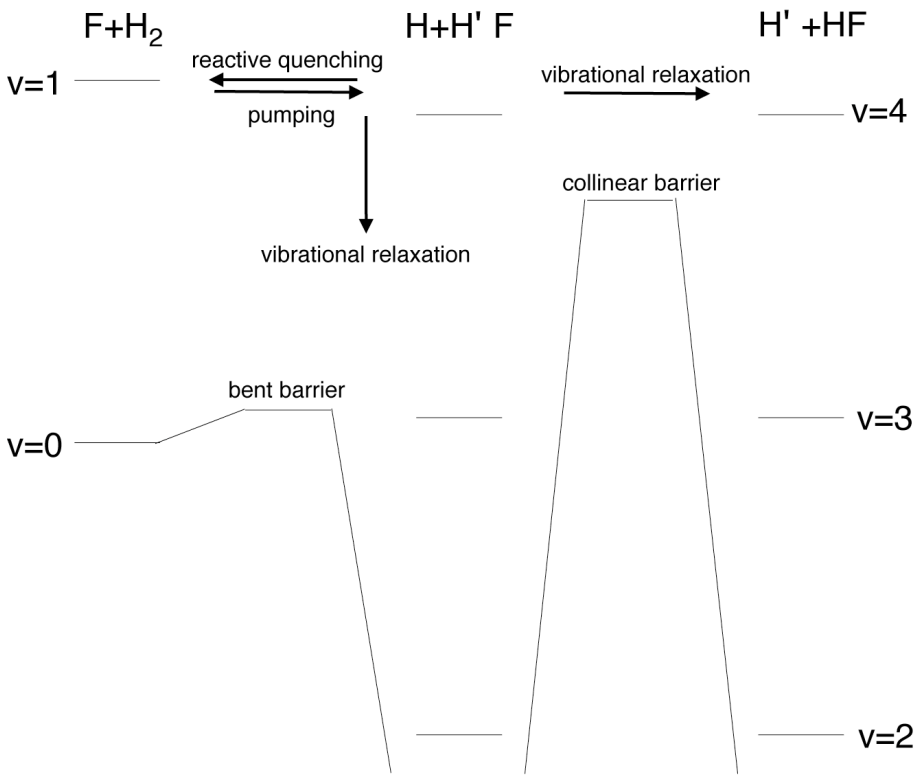

Figure 2.1 Schematic plot of the energetics of the three channels relevant to the vibrational relaxation of HF(v). The relative reactant energies, the position of the barriers and wells, and the position of the indicated $F+H_2$ and $H+H'F$ channels have been drawn to scale.

The actual topology of the linear saddle points for the $H'+HF \rightarrow H+H'F$ and $H'+HF \rightarrow H_2+F$ reactions is illustrated by Figs. 2.2 and 2.3. Here, we plot the potential energy surface as the function of the bond coordinates R_{FH} and $R_{FH'}$ (or $R_{HH'}$). The asymptotic reactant or product arrangements correspond to the situation where one of the bond coordinates is large while the other is equal to the equilibrium internuclear separation of either HF or H_2.

If we start at a point A corresponding to reactants at large separation and let R_{FH} decrease, the energy steadily increases if $R_{FH'}$ (or $R_{HH'}$) is more or less constant. It is as though we were traveling up a valley. However, motion in a perpendicular direction results in a rapid increase in energy. If we continue along the bottom of the valley, following the minimum energy pathway, the energy continues to increase until we reach point B, which is a saddle point. Motion forwards or backwards along the minimum energy path results in a decrease in energy but motion in a perpendicular direction results in a very large increase in energy. The saddle point B corresponds to the top of the activation barrier in simple transition state theory. The valley leading up to the saddle point is known as the entrance channel. Continuation along the minimum energy path from the saddle point results in a steady decrease in energy along the exit channel until one reaches the asymptotic product arrangement at large separation (point C).

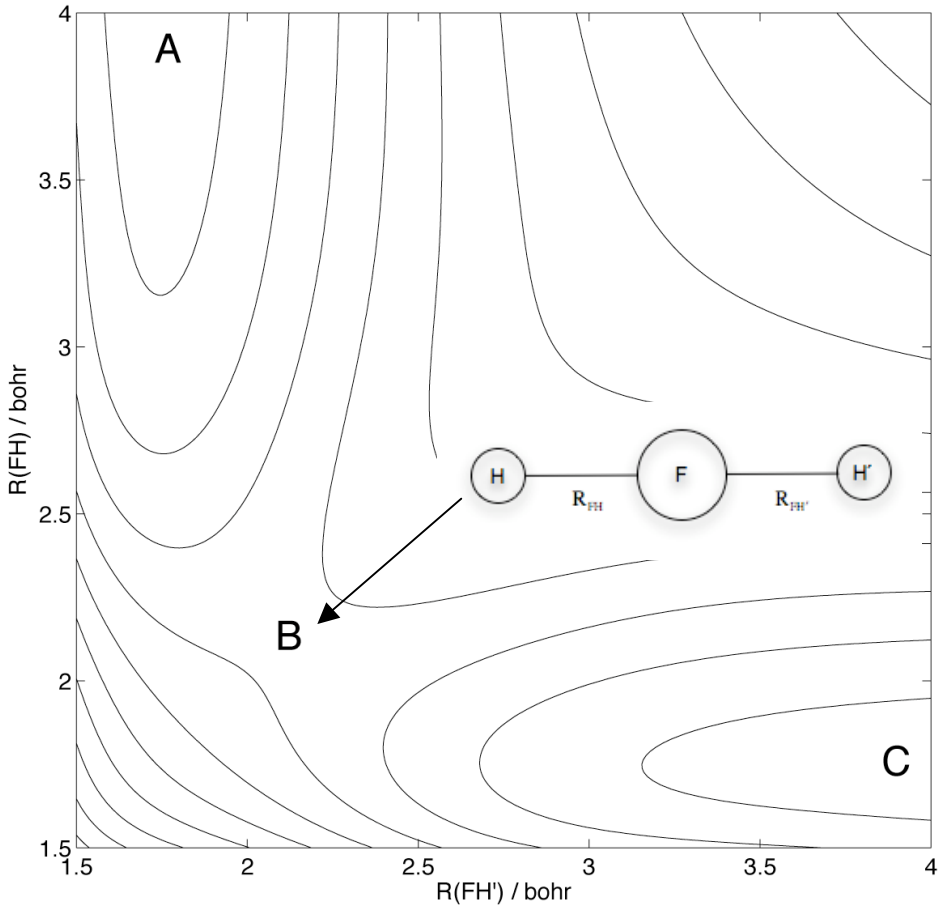

Figure 2.2 Contour plot of the potential energy surface for collinear HFH′, starting from the entrance channel A, passing through the energy barrier B and ending along the exit channel C

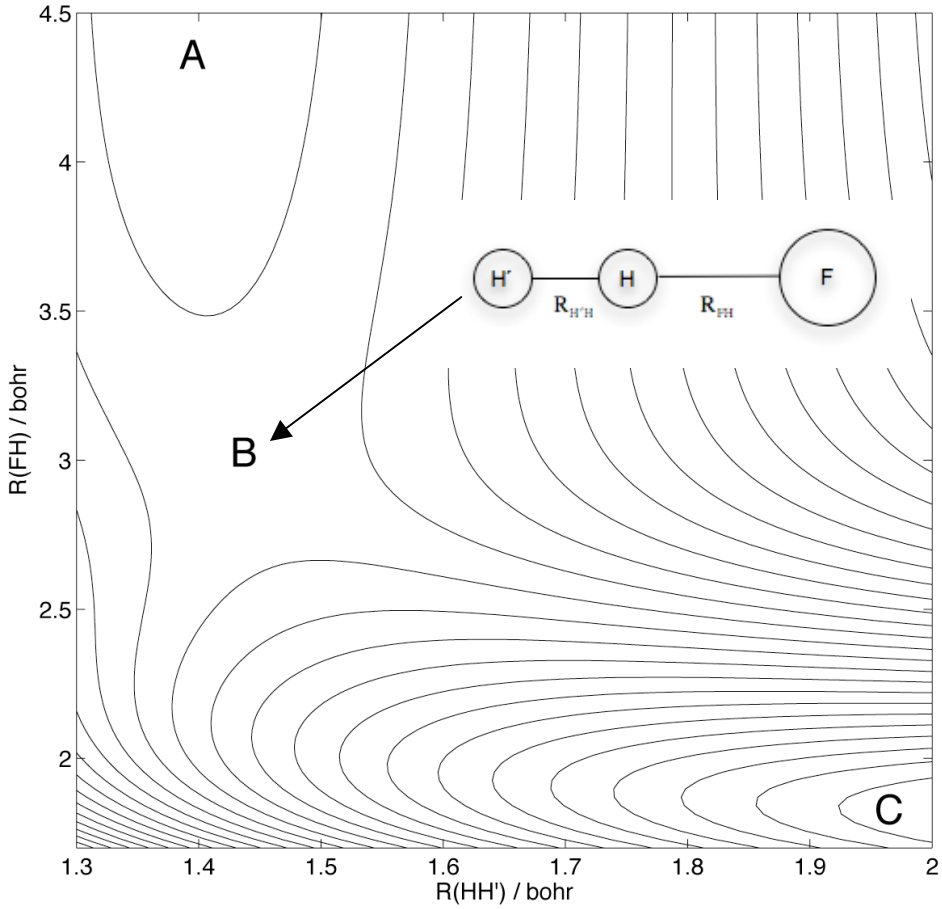

Figure 2.3 Contour plot of the potential energy surface for collinear FHH′, starting from the entrance channel A, passing through the energy barrier B and ending along the exit channel C

Chapter 3: Treatment of the dynamics

The quantum reactive scattering calculations are carried out in a manner similar to the recent work of Manolopoulos and co-workers on the $F+H_2$ [18,19] and $F+HD$ [20] reactions. We use a close-coupled, time-independent method[21-24] based on the use of Delves hyperspherical coordinates.[25] We assume that the Born-Oppenheimer approximation between the electron and nuclear motions is valid and that the ground- state potential energy surface is known. All interactions involving nuclear and electronic spins and nuclear and electronic orbital angular momenta are neglected**.** The wave function for the nuclear motion (the scattering wavefunction) is expanded in a truncated parity-adapted basis set of products of vibrational-rotational states for each of three arrangement channels in the body-fixed frame.[22,24,26]

By expansion in a basis, the Schrödinger equation for the motion of the three nuclei, which is a partial differential equation in the three internal degrees of freedom, becomes converted to a set of coupled ordinary 2^{nd} order differential equations. Numerical solution of these "closed-coupled" (or "coupled-channel") equations is carried out by propagation from small to large hyperradius through a series of sectors. Canonical orthogonalization is then used to construct a set of orthogonal basis functions (called surface functions) in each sector. To solve the close-coupled equations, we use the ABC code of Manolopoulos and co-workers.[24]

In the following sections, we shall present a few details about use of the coupled-channel (CC) method in heavy-particle collisions including energy transfer.

In particular, we shall explain how to construct the definite parity basis based on the symmetric property of the H-F-H potential, as well as the method used to separate the three different product channels in order to compare with the experimental measurement.

3.1. Coupled Schrödinger Equations and Basis Functions in Space and Body-fixed Frames

In Fig. 3.1 we show how the three-dimensional internal configuration space can be naturally divided into arrangement channel region subspaces, labeled by the indices $\alpha = 1,2,3$, with $\alpha = 1$ for A+BC, $\alpha = 2$ for B+CA and $\alpha = 3$ for C+AB. In our particular case, the labels A, B and C correspond to F, H and H′ atoms. In each arrangement subspace we use Jacobi coordinates, which are defined by[22,23,26] $\vec{\mathcal{R}}_\alpha$, the vector from the center of mass of the diatomic moiety to the atom, which describes the asymptotic translational motion; $\vec{r}_\alpha$, the bond axis of the diatomic moiety, which describes the vibrational and rotational motions of the diatomic moiety; and γ_α, the angle between $\vec{\mathcal{R}}_\alpha$ and $\vec{r}_\alpha$, with $\gamma_\alpha = \cos^{-1}(\vec{\mathcal{R}}_\alpha \cdot \vec{r}_\alpha)$.

In arrangement 3 for example, the Schrödinger equation for the motion of the three nuclei is[23]

$$\left(-\frac{\hbar^2}{2\mu_{C,AB}} \nabla^2_{\vec{\mathcal{R}}_3} - \frac{\hbar^2}{2\mu_{AB}} \nabla^2_{\vec{r}_3} + V(\mathcal{R}_3, r_3, \gamma_3) - E \right) \Psi(\vec{\mathcal{R}}_3, \vec{r}_3) = 0 \qquad (3.1)$$

where $\mu_{C,AB}$ and μ_{AB} are reduced masses

$$\mu_{AB} = \frac{m_A m_B}{m_A + m_B} \qquad \mu_{C,AB} = \frac{m_C (m_A + m_B)}{m_A + m_B + m_C} \tag{3.2}$$

We then define the mass-scaled Jacobi coordinates[27] in terms of $\vec{\mathcal{R}}_\alpha$ and $\vec{r}_\alpha$ by

$R_\alpha = d_\alpha \mathcal{R}_\alpha$, $r_\alpha = d_\alpha r_\alpha$

where, for α=3, $$d_{\alpha=3} = \left(\frac{\mu_{C,AB}}{\mu_{AB}} \right)^{1/4} \tag{3.3}$$

Then the Schrödinger equation becomes[23]

$$\left(-\frac{\hbar^2}{2\mu} \left(\nabla^2_{R_\alpha} + \nabla^2_{r_\alpha} \right) + V(R_\alpha, r_\alpha, \gamma_\alpha) - E \right) \Psi(\overrightarrow{R_\alpha}, \overrightarrow{r_\alpha}) = 0 \tag{3.4}$$

The advantage in using mass-scaled coordinates is the appearance of a single reduced mass μ which is independent of the choice of arrangement

$$\mu = \left(\frac{m_A m_B m_C}{m_A + m_B + m_C} \right)^{1/2} \tag{3.5}$$

In a space-fixed frame,[23,26] the spherical polar coordinates for the vectors $\overrightarrow{R_\alpha}, \overrightarrow{r_\alpha}$ are $(R_\alpha, \theta_{R_\alpha}, \phi_{R_\alpha})$ and $(r_\alpha, \theta_{r_\alpha}, \phi_{r_\alpha})$. If we express the Laplacian operators in terms of R_α, r_α and these angles, the Schrödinger equation can be written in terms of the rotational angular momentum operator $\hat{j}$ and orbital angular momentum operator $\hat{l}$

$$\left[-\frac{\hbar^2}{2\mu} \left(\frac{1}{R_\alpha} \frac{\partial^2}{\partial R_\alpha^2} R_\alpha + \frac{1}{r_\alpha} \frac{\partial^2}{\partial r_\alpha^2} r_\alpha \right) + \frac{\hat{j_\alpha}^2}{2\mu r_\alpha^2} + \frac{\hat{l_\alpha}^2}{2\mu R_\alpha^2} + V(R_\alpha, r_\alpha, \gamma_\alpha) - E \right] \Psi(\overrightarrow{R_\alpha}, \overrightarrow{r_\alpha}) = 0 \tag{3.6}$$

The total angular momentum operator $\hat{J}$ is the vector sum of $\hat{j}$ and $\hat{l}$. Both its magnitude and space fixed projection M are conserved during the collision, independent of arrangement channel.

The full space-fixed wavefunctions are then expanded as[22,23]

$$\Psi_{JM}(\overrightarrow{R_\alpha},\overrightarrow{r_\alpha}) = \sum_{l_\alpha j_\alpha} \varphi^{JM}_{l_\alpha j_\alpha}(\theta_{R_\alpha},\phi_{R_\alpha};\theta_{r_\alpha},\phi_{r_\alpha}) G^{JM}_{l_\alpha j_\alpha}(R_\alpha,r_\alpha) \tag{3.7}$$

$$\varphi^{JM}_{l_\alpha j_\alpha}(\theta_{R_\alpha},\phi_{R_\alpha};\theta_{r_\alpha},\phi_{r_\alpha}) = \sum_{m_{j\alpha},m_{l\alpha}} C(j_\alpha l_\alpha J; m_{j_\alpha} m_{l_\alpha} M) Y_{l_\alpha m_{l_\alpha}}(\theta_{R_\alpha},\phi_{R_\alpha}) Y_{j_\alpha m_{j_\alpha}}(\theta_{r_\alpha},\phi_{r_\alpha}) \tag{3.8}$$

where $C(jlJ;mmM)$ is a Clebsch-Gordan coefficient;[28] Y_{jm} is a spherical harmonic;[28] and M and m are the projection quantum numbers of the angular momenta along the space-fixed OZ axis.

We now introduce a body-fixed coordinate system[23] OX′Y′Z′ as shown in Fig. 3.2. The variables used to describe the system are $R_\alpha,\theta_{R_\alpha},\phi_{R_\alpha},r_\alpha,\gamma_\alpha,\psi_\alpha$, as compared to $R_\alpha,\theta_{R_\alpha},\phi_{R_\alpha},r_\alpha,\theta_{r_\alpha},\phi_{r_\alpha}$ in the space-fixed frame. Here, ψ_α is defined as the angle between the two planes OXZ and OX′Z′. A motion in which the variables $R_\alpha,\theta_{R_\alpha},\phi_{R_\alpha},r_\alpha,\gamma_\alpha$ are kept constant but ψ_α varies corresponds to a "tumbling" of the triatomic system around the vector $\vec{R}$. For this reason ψ_α will be called the tumbling angle.

The overall rotational motion is described by the quantum numbers j and k, where the associated tumbling quantum number k specifies the component of the total angular momentum $\hat{J}$ around the body-frame OZ′ axis. Since the component of the orbital angular momentum $\hat{l}$ around this axis vanishes, k also specifies the z

component of rotational angular momentum $\hat{j}$ in the body-fixed frame. In reactive scattering calculations, where the designation of the z axis depends on the arrangement (F–H_2, HF–H′, or H′F–H), the body-frame projection differs from one arrangement to another. In the ABC code,[24] which we use to solve the Schrödinger equations for the A+BC dynamics, this is called the helicity quantum number.

The rotationally coupled body-fixed basis functions can be defined in terms of Wigner rotation matrix elements D^J_{Mk} [28] similarly to Eq. (3.7) and (3.8). We have [22,23]

$$\Psi_{JM}(\overrightarrow{R_\alpha},\overrightarrow{r_\alpha}) = \sum_{k_\alpha=-J}^{J} D^J_{Mk_\alpha}(\phi_{R_\alpha},\theta_{R_\alpha},0)\Phi_{Jk_\alpha}(R_\alpha,r_\alpha,\gamma_\alpha,\psi_\alpha) \tag{3.9}$$

$$\Phi_{Jk_\alpha}(R_\alpha,r_\alpha,\gamma_\alpha,\psi_\alpha) = \sum_{j_\alpha=|k_\alpha|}^{\infty} Y_{j_\alpha k_\alpha}(\gamma_\alpha,\psi_\alpha) w_{Jj_\alpha k_\alpha}(R_\alpha,r_\alpha);\ k_\alpha = -J,-J+1,...,J;\ J=0,1,2,... \tag{3.10}$$

We combine Eqs. (3.9) and (3.10), and further separate the two nuclear distance variables R and r by expanding in a complete set of functions $\phi_{vj}(r)$ which span the vibrational motion of the diatomic moiety. We then write the full basis functions for the triatomic system (ABC) in the body-fixed frame as:[23]

$$\begin{aligned}\Psi_{JM}(\overrightarrow{R_\alpha},\overrightarrow{r_\alpha}) &= \sum_{k_\alpha=-J}^{J}\sum_{j_\alpha=|k_\alpha|}^{\infty} D^J_{Mk_\alpha}(\phi_{R_\alpha},\theta_{R_\alpha},0) Y_{j_\alpha k_\alpha}(\gamma_\alpha,\psi_\alpha) w^J_{j_\alpha k_\alpha}(R_\alpha,r_\alpha) \\ &= \sum_{k_\alpha=-J}^{J}\sum_{j_\alpha=|k_\alpha|}^{\infty}\sum_{v_\alpha} D^J_{Mk_\alpha}(\phi_{R_\alpha},\theta_{R_\alpha},0) Y_{j_\alpha k_\alpha}(\gamma_\alpha,\psi_\alpha) g^{Jk_\alpha}_{v_\alpha j_\alpha}(R_\alpha)\frac{\phi_{v_\alpha j_\alpha}(r_\alpha)}{R_\alpha r_\alpha}\end{aligned} \tag{3.11}$$

where $g_{vj}^{Jk}(R)$ describes the stretch of the HF-H complex, and $Y_{jk}(\gamma,\psi)$ is a spherical harmonic. One may show[23] that the body-fixed and space-fixed representations may be related by using the equality

$$D^{J}_{Mk_\alpha}(\phi_\alpha,\theta_\alpha,0)Y_{j_\alpha k_\alpha}(\gamma_\alpha,\psi_\alpha)=\left(\frac{4\pi}{2J+1}\right)^{1/2}\sum_{l_\alpha}(-1)^{j_\alpha-k_\alpha}C(Jj_\alpha l_\alpha;k_\alpha-k_\alpha 0)\varphi^{JM}_{l_\alpha j_\alpha}(\theta_{R_\alpha},\phi_{R_\alpha};\theta_{r_\alpha},\phi_{r_\alpha}) \tag{3.12}$$

Both the body-fixed and space-fixed formalisms lead to the same number of coupled equations. In a body-fixed coordinate system, the matrix of the potential in Eq. (3.6) is diagonal in the helicity quantum number within a particular arrangement. This simplification is useful in the development of approximate theories. However, the orbital angular momentum l in this helicity frame is no longer a good quantum number, since the matrix of $\hat{l}^2$ is no longer diagonal.

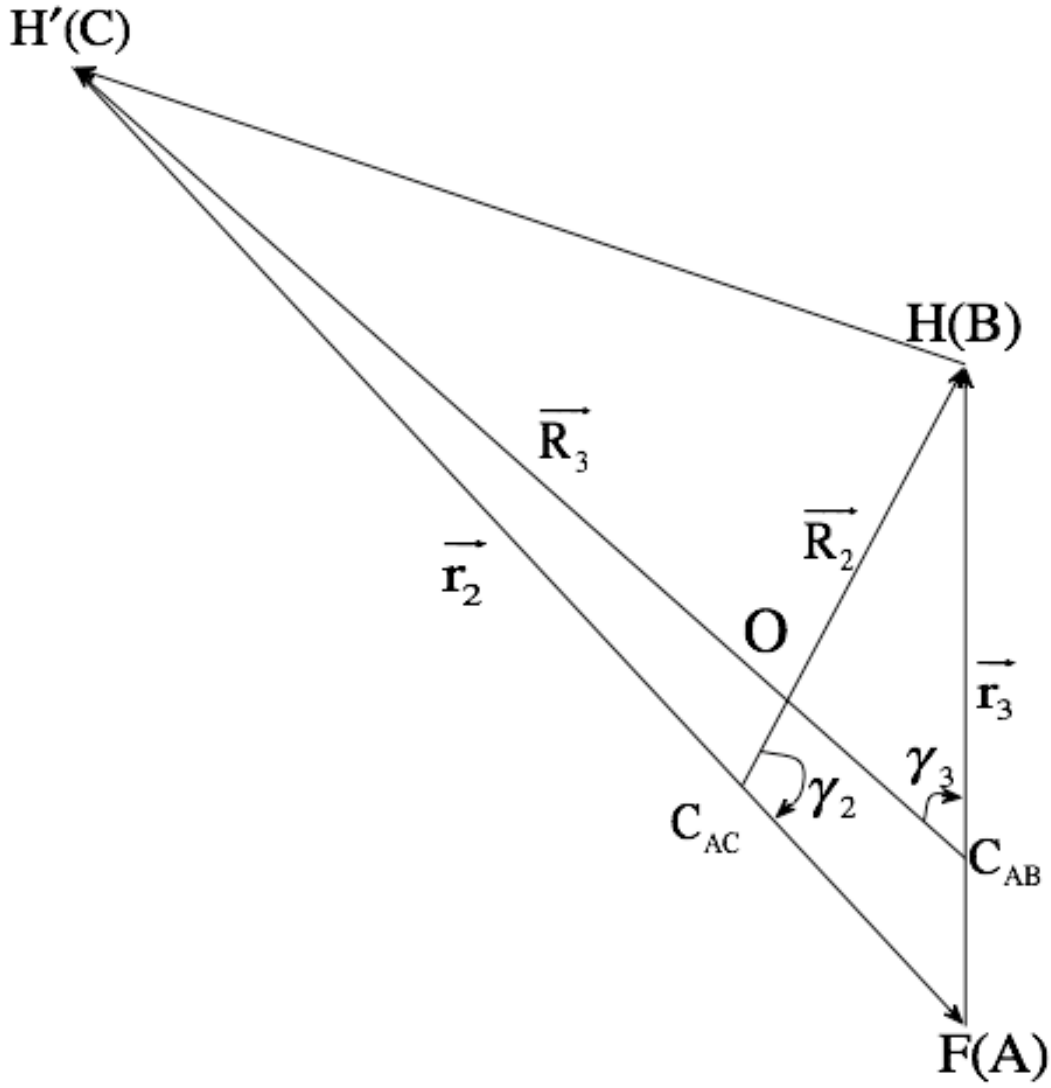

Figure 3.1 Vector plots showing the locations of the three atoms A, B and C relative to the center of mass O; C_{AB} and C_{AC} denote the locations of the center of mass of diatoms AB and AC. Also γ_2 is the bending angle between $\vec{R}_2$ and $\vec{r}_2$ while γ_3 is the bending angle between $\vec{R}_3$ and $\vec{r}_3$. The $\vec{R}_1$, $\vec{r}_1$ and γ_1 are not shown in this figure.

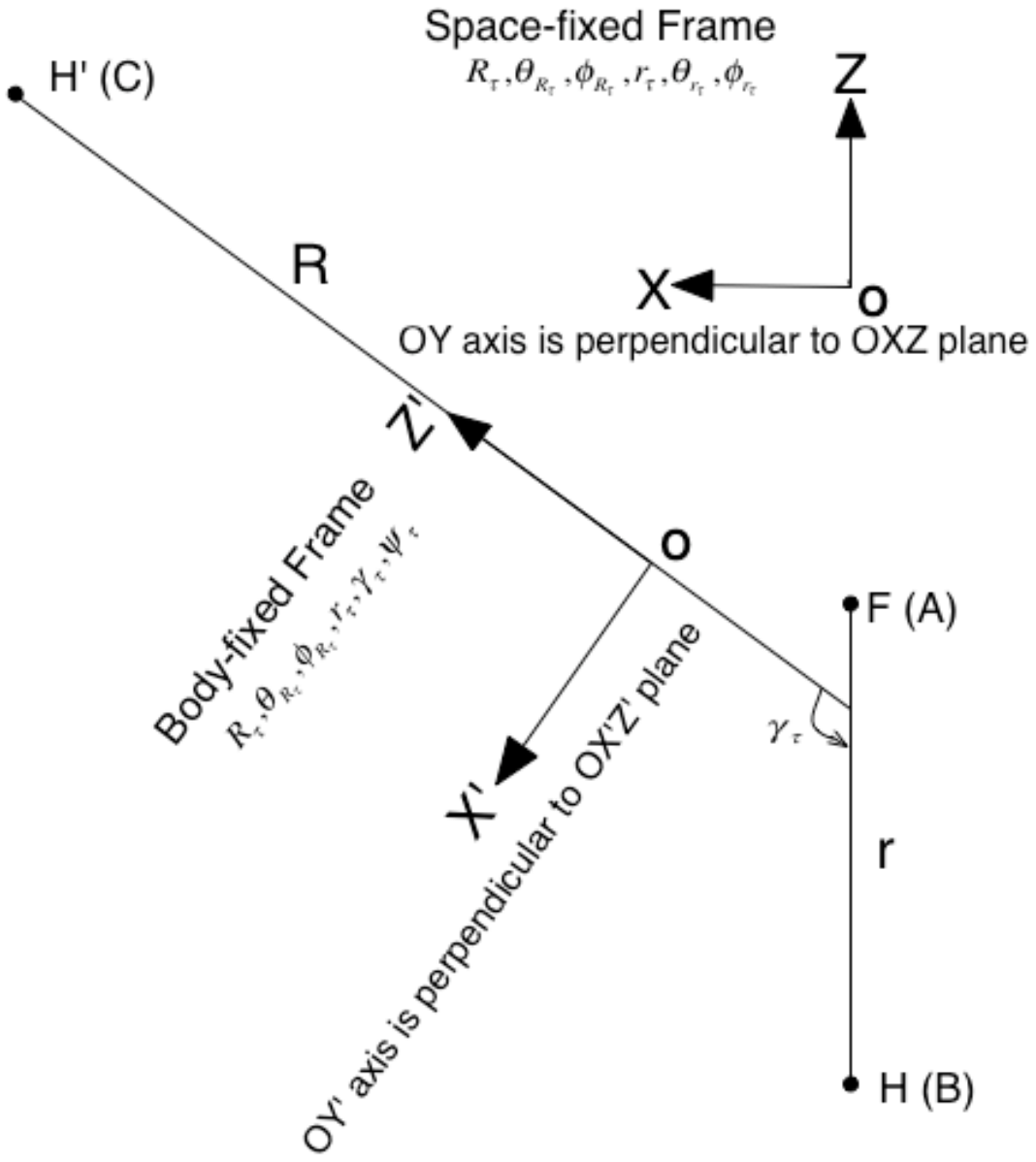

Figure 3.2 Plot of the ABC triatomic system in the space-fixed OXY and body-fixed OX′Y′Z′ frames. The variables used to describe the system in the body-fixed frame are $R_\tau, \theta_{R_\tau}, \phi_{R_\tau}, r_\tau, \gamma_\tau, \psi_\tau$, which should be compared to $R_\tau, \theta_{R_\tau}, \phi_{R_\tau}, r_\tau, \theta_{r_\tau}, \phi_{r_\tau}$ in the space-fixed frame

3.2. Triatomic parity and definite parity basis

The inversion operator commutes with the Hamiltonian for the triatomic system. Therefore, we are free to choose basis functions which are eigenfunctions of the inversion operator $\hat{I}$ with eigenvalues ±1. If we use body-fixed variables $\vec{R_\alpha}$ and $\vec{r_\alpha}$ to express the triatomic wave function as $\Psi_{JM}(\vec{R_\alpha},\vec{r_\alpha})$, the action of the inversion operation can be shown to be:

$$\hat{I}\Psi_{JM}(R_\alpha,\theta_{R_\alpha},\phi_{R_\alpha},r_\alpha,\gamma_\alpha,\psi_\alpha)=\Psi_{JM}(R_\alpha,\pi-\theta_{R_\alpha},\pi+\phi_{R_\alpha},r_\alpha,\gamma_\alpha,\pi-\psi_\alpha) \tag{3.13}$$

The body-fixed basis functions are given by Eq. (3.11). Using the relationships[29]

$$D^J_{Mk_\alpha}(\phi_{R_\alpha}+\pi,\pi-\theta_{R_\alpha},0)=(-1)^J D^J_{M,-k_\alpha}(\phi_{R_\alpha},\theta_{R_\alpha},0) \tag{3.14}$$

$$Y_{j_\alpha k_\alpha}(\gamma_\alpha,\pi-\psi_\alpha)=Y_{j_\alpha,-k_\alpha}(\gamma_\alpha,\psi_\alpha) \tag{3.15}$$

and changing the sign of k_α, we find

$$\hat{I}\Psi_{JM}(\vec{R_\alpha},\vec{r_\alpha})=(-1)^J\sum_{k_\alpha=-J}^{J}\sum_{j_\alpha=|k_\alpha|}^{\infty}\sum_{v_\alpha}D^J_{Mk_\alpha}(\phi_{R_\alpha},\theta_{R_\alpha},0)Y_{j_\alpha k_\alpha}(\gamma_\alpha,\psi_\alpha)g^{J-k_\alpha}_{v_\alpha j_\alpha}(R_\alpha)\frac{\phi_{v_\alpha j_\alpha}(r_\alpha)}{r_\alpha R_\alpha}=\Psi_{JM}(-\vec{R_\alpha},-\vec{r_\alpha}) \tag{3.16}$$

This result indicates that $\Psi_{JM}(\vec{R_\alpha},\vec{r_\alpha})$ is not an eigenfunction of the parity operator $\hat{I}$ unless $J=0$.

Since $\hat{I}$ commutes with the Hamiltonian, we can take linear combination of $\Psi_{JM}(\vec{R_\alpha},\vec{r_\alpha})$s to create simultaneous eigenfunctions of $\hat{I}$ and the Hamiltonian, namely

$$\Psi^P_{JM}(\vec{R_\alpha},\vec{r_\alpha})=\frac{1}{\sqrt{2}}\left\{\Psi_{JM}(\vec{R_\alpha},\vec{r_\alpha})+P\Psi_{JM}(-\vec{R_\alpha},-\vec{r_\alpha})\right\} \tag{3.17}$$

where $P=\pm1$. From Eq. (3.16), we see that

$$\hat{I}\Psi^{P}_{JM}(\vec{R}_\alpha,\vec{r}_\alpha) = (-1)^J P\Psi^{P}_{JM}(\vec{R}_\alpha,\vec{r}_\alpha) \tag{3.18}$$

Thus by constructing parity eigenfunctions, we can separate our coupled Schrödinger equations into two uncoupled sets – those with parity $(-1)^J$ and those with parity $-(-1)^J$. Using this triatomic parity decoupling method, we define the triatomic parity eigenvalue $P=\pm(-1)^J$, and calculate the parity-adapted S-matrix elements $S^{J,P}_{\alpha vjk,\alpha' v' j' k'}$, where k and k' are the initial and final helicity quantum numbers. In the ABC code, k and k' are restricted such that $0 \le k \le \min(J,j)$ and $0 \le k' \le \min(J,j')$, while $k=0$ and $k'=0$ only occur in the parity block with $P=(-1)^J$. The unprimed and primed quantities refer to the initial and final states, while the label α designates the arrangement with α=1 for A+BC, α=2 for B+CA and α=3 for C+AB.

After determining the S matrix we can convert the parity-adapted S-matrix elements $S^{J,P}_{\alpha vjk,\alpha' v' j' k'}$ into standard helicity-representation S-matrix elements $S^{J}_{\alpha vjk,\alpha' v' j' k'}$ using the formulas[24]

$$S^{J}_{\alpha vjk,\alpha' v' j' k'} = S^{J}_{\alpha' v' j' -k',\alpha vj-k} = \begin{Bmatrix} \frac{1}{2}\left[S^{J,+1}_{\alpha vjk,\alpha' v' j' k'} + S^{J,-1}_{\alpha vjk,\alpha' v' j' k'}\right] & (k=0 \text{ and } k'=0) \\ \frac{1}{\sqrt{2}}\left[S^{J,+1}_{\alpha vjk,\alpha' v' j' k'} + S^{J,-1}_{\alpha vjk,\alpha s v' j' k'}\right] & (k\neq 0 \;\; k'=0 \text{ or } k=0 \;\; k'\neq 0) \\ S^{J,+1}_{\alpha vjk,\alpha' v' j' k'} + S^{J,-1}_{\alpha vjk,\alpha' v' j' k'} & (k\neq 0 \text{ and } k'\neq 0) \end{Bmatrix} \tag{3.19}$$

and

$$S^{J}_{\alpha v j-k,\alpha' v' j' k'} = S^{J}_{\alpha' v' j' k',\alpha v j-k} = (-1)^{J} \begin{Bmatrix} \frac{1}{2}\left[S^{J,+1}_{\alpha v j k,\alpha' v' j' k'} - S^{J,-1}_{\alpha v j k,\alpha' v' j' k'} \right] & (k = 0 \text{ and } k' = 0) \\ \frac{1}{\sqrt{2}}\left[S^{J,+1}_{\alpha v j k,\alpha' v' j' k'} - S^{J,-1}_{\alpha v j k,\alpha' v' j' k'} \right] & (k \neq 0 \;\; k' = 0 \text{ or } k = 0 \;\; k' \neq 0) \\ S^{J,+1}_{\alpha v j k,\alpha' v' j' k'} - S^{J,-1}_{\alpha v j k,\alpha' v' j' k'} & (k \neq 0 \text{ and } k' \neq 0) \end{Bmatrix} \tag{3.20}$$

3.3. Diatomic parity and permutation symmetry

In addition, the permutation symmetry in $H'+HF \rightarrow H'+HF$ and $H'+HF \rightarrow H+H'F$ reactions can be used to reduce the number of basis functions that must be simultaneously considered. The FH_2 potential energy is symmetric with respect to interchange of the two hydrogen atoms, namely V(F,H,H′)=V(F,H′,H). To exploit this symmetry, we expand the wavefunction for the system as the symmetric and antisymmetric linear combinations of the primitive basis functions

$$\Psi_p(\mathrm{F,H,H'}) = \frac{1}{\sqrt{2}}\left[\Psi(\mathrm{F,H,H'}) + p\Psi(\mathrm{F,H',H})\right] \tag{3.21}$$

where p = ±1. Because the Hamiltonian is invariant with respect to H-atom interchange, there will be no coupling between the symmetric (p = 1) and antisymmetric (p = –1) states, so that the coupled scattering equations are further reduced in size by a factor of ≈2.

In practice, in the $F+H_2$ arrangement, the triatomic wavefunction is expanded in the basis functions

$$|JMK\mathrm{v}jk\rangle = \frac{1}{r_1}\left(\frac{2J+1}{4\pi}\right)^{1/2} D^{J*}_{Mk}(\phi_1,\theta_1,0)Y_{jk}(\gamma_1,\psi_1)\phi_{\mathrm{v}j}(r_1) \tag{3.22}$$

where Y_{jk} describes the rotational, and $\frac{1}{r}\phi_{\mathrm{v}j}$ the vibrational, motion of the H_2 moiety. The vibrational wavefunctions $\phi_{\mathrm{v}j}$ are symmetric with respect to $\mathrm{H} \leftrightarrow \mathrm{H}'$ exchange. This exchange corresponds to an inversion of the coordinate system of the H_2 molecule, so that the rotational wavefunctions have the symmetry

$$\widehat{P_{\mathrm{HH}'}}Y_{jk}(\gamma,0) = (-1)^j Y_{jk}(\gamma,0) \tag{3.23}$$

Thus, for the F+H_2 arrangement, the symmetric basis functions include only even-*j* terms, and the antisymmetric basis functions, only odd-*j* terms.

For the HF+H′ and H′F+H arrangements, the wavefunctions are expanded in basis functions similar to Eq.3.22, which we designate

$$|JMK\mathrm{v}jk,\mathrm{H}\rangle = \frac{1}{r_2}\left(\frac{2J+1}{4\pi}\right)^{1/2} D^{J*}_{Mk}(\phi_2,\theta_2,0)Y_{jk}(\gamma_2,\psi_2)\phi_{\mathrm{v}j}(r_2) \tag{3.24}$$

and

$$|JMK\mathrm{v}jk,\mathrm{H}'\rangle = \frac{1}{r_3}\left(\frac{2J+1}{4\pi}\right)^{1/2} D^{J*}_{Mk}(\phi_3,\theta_3,0)Y_{jk}(\gamma_3,\psi_3)\phi_{\mathrm{v}j}(r_3) \tag{3.25}$$

where the subscripts "2" and "3" refer, respectively, to the HF+H′ and H′F+H arrangements. Taking the permutation symmetry into consideration, as outlined in Eq. (3.21), we use linear combinations of the arrangement "2" and arrangement "3" basis functions

$$|JMK\mathrm{v}jk,p\rangle = \frac{1}{\sqrt{2}}\left[|JMK\mathrm{v}jk,\mathrm{HF}\rangle + p|JMK\mathrm{v}jk,\mathrm{H}'\mathrm{F}\rangle\right] \tag{3.26}$$

In the ABC code, which we use for our calculations, the interchange index $p = (-1)^j$ is called *jpar*. Thus in the calculations, if the parameter *jpar* is +1, the total wavefunction is expanded in the symmetric (even j) functions for the F+H_2 arrangement and the symmetric linear combination of H′F+H and HF+H′ basis functions; if *jpar* = −1, the odd j F + H_2 and antisymmetric F+HF linear combination are used [Eq.(3.26)].

Each scattering calculation yields a parity- and interchange-adapted S matrix, with elements $S^{J,P,p}_{\mathrm{v}jk,\mathrm{v}'j'k'}$. The square of the S matrix element corresponds to the transition probability. Suppose we are interested in HF+H→HF+H inelastic scattering, either with or without H-atom exchange. Since the H atoms are indistinguishable, an experiment would measure the inelastic probability

$$P^{J,P}(\mathrm{v}jk \to \mathrm{v}'j'k') = \left|S^{J,P,+1}_{\mathrm{v}jk,\mathrm{v}'j'k'}\right|^2 + \left|S^{J,P,-1}_{\mathrm{v}jk,\mathrm{v}'j'k'}\right|^2 \tag{3.27}$$

Note that there are no cross terms in Eq. (3.27), because the interchange symmetry label p is a good quantum number. Scattering of the +1 states and scattering of the −1 states occurs independently. The total inelastic probability is the sum of the probability associated with inelastic scattering of the +1 states added to the probability associated with inelastic scattering of the −1 states.

Experimentally, is impossible to distinguish between those inelastic collisions which exchange, and those which do not exchange, the two H atoms. However, as theoreticians we can make this distinction. From Eq. (3.26), we see the distinguishable atom wavefunction can be written in terms of the symmetrized basis functions as followings:

$$|JMK\mathrm{v}jk,\mathrm{HF}\rangle = \frac{1}{\sqrt{2}}\left[|JMK\mathrm{v}jk,+1\rangle + |JMK\mathrm{v}jk,-1\rangle\right] \tag{3.28a}$$

and

$$|JMK\mathrm{v}jk,\mathrm{H'F}\rangle = \frac{1}{\sqrt{2}}\left[|JMK\mathrm{v}jk,+1\rangle - |JMK\mathrm{v}jk,-1\rangle\right] \tag{3.28b}$$

Consequently, the amplitude for the collision-induced transition for a non-H-atom exchanging transition from an initial H′+HF(vjk) state to a final H′+HF(v′$j'k'$) state is

$$A^{J,P}(\mathrm{HF},\mathrm{v}jk \rightarrow \mathrm{HF},\mathrm{v}'j'k') = A^{J,P}(\mathrm{H'F},\mathrm{v}jk \rightarrow \mathrm{H'F},\mathrm{v}'j'k') = \frac{1}{2}\left[S^{J,P,+1}_{\mathrm{v}jk,\mathrm{v}'j'k'} + S^{J,P,-1}_{\mathrm{v}jk,\mathrm{v}'j'k'}\right] \tag{3.29}$$

The amplitude is identical for the H+H′F(vjk) → H+H′F(v′j′k′) transition. Similarly, the amplitude for the collision-induced HF(vjk) → H′F(v′$j'k'$) transition is

$$A^{J,P}(\mathrm{HF},\mathrm{v}jk \rightarrow \mathrm{H'F},\mathrm{v}'j'k') = A^{J,P}(\mathrm{H'F},\mathrm{v}jk \rightarrow \mathrm{HF},\mathrm{v}'j'k') = \frac{1}{2}\left[S^{J,P,+1}_{\mathrm{v}jk,\mathrm{v}'j'k'} - S^{J,P,-1}_{\mathrm{v}jk,\mathrm{v}'j'k'}\right] \tag{3.30}$$

Thus, at the level of the *S*-matrix elements, the amplitudes for the non-atom-exchanging and atom-exchanging inelastic transitions are the positive and negative combinations of the two corresponding definite-exchange-symmetry *S*-matrix elements. The corresponding transition probabilities are:

$$P^{J,P}(\mathrm{HF},\mathrm{v}jk \rightarrow \mathrm{HF},\mathrm{v}'j'k') = P^{J,P}(\mathrm{H'F},\mathrm{v}jk \rightarrow \mathrm{H'F},\mathrm{v}'j'k') = \frac{1}{4}\left[\left|S^{J,P,+1}\right|^2 + \left|S^{J,P,-1}\right|^2 + 2\,\mathrm{Re}\left(S^{J,P,+1*}S^{J,P,-1}\right)\right] \tag{3.31}$$

and

$$P^{J,P}(\mathrm{HF},\mathrm{v}jk \rightarrow \mathrm{H'F},\mathrm{v}'j'k') = P^{J,P}(\mathrm{H'F},\mathrm{v}jk \rightarrow \mathrm{HF},\mathrm{v}'j'k') = \frac{1}{4}\left[\left|S^{J,P,+1}\right|^2 + \left|S^{J,P,-1}\right|^2 - 2\,\mathrm{Re}\left(S^{J,P,+1*}S^{J,P,-1}\right)\right] \tag{3.32}$$

If we add Eqs. (3.31) and (3.32) and multiply by 2, we obtain Eq. (3.27).

Thus, the experimentally measurable inelastic probability [Eq.(3.27)] is equivalent to the sum of the two distinguishable atom direct probabilities ($\mathrm{HF} \rightarrow \mathrm{HF}$ and $\mathrm{H'F} \rightarrow \mathrm{H'F}$) plus the two distinguishable-atom exchange processes ($\mathrm{HF} \rightarrow \mathrm{H'F}$ and $\mathrm{H'F} \rightarrow \mathrm{HF}$).

We can subsequently define a total "direct" and total "exchange" probability as follows:

$$P_D^{J,P}(\mathrm{v}jk \rightarrow \mathrm{v'}j'k') = P^{J,P}(\mathrm{HF}, \mathrm{v}jk \rightarrow \mathrm{HF}, \mathrm{v'}j'k') + P^{J,P}(\mathrm{H'F}, \mathrm{v}jk \rightarrow \mathrm{H'F}, \mathrm{v'}j'k')$$
$$= \frac{1}{2}\left[\left|S^{J,P,+1}\right|^2 + \left|S^{J,P,-1}\right|^2 + 2\,\mathrm{Re}\left(S^{J,P,+1*}S^{J,P,-1}\right)\right] \tag{3.33}$$

$$P_E^{J,P}(\mathrm{v}jk \rightarrow \mathrm{v'}j'k') = P^{J,P}(\mathrm{HF}, vjk \rightarrow \mathrm{H'F}, \mathrm{v'}j'k') + P^{J,P}(\mathrm{H'F}, \mathrm{v}jk \rightarrow \mathrm{HF}, \mathrm{v'}j'k')$$
$$= \frac{1}{2}\left[\left|S^{J,P,+1}\right|^2 + \left|S^{J,P,-1}\right|^2 - 2\,\mathrm{Re}\left(S^{J,P,+1*}S^{J,P,-1}\right)\right] \tag{3.34}$$

3.4. Integral cross sections, Cumulative reaction probabilities, State-to-state rate constants and Vibrational relaxation rate constants

3.4.1. Integral cross sections

We are interested in calculating state-resolved integral cross sections $\sigma_{\mathrm{v},j\rightarrow\mathrm{v'},j'}(E_C)$ and overall integral removal cross section $\sigma_{\mathrm{v}j}(E_C)$ as the functions of collision energy E_C for three channels: $\mathrm{H'+HF(v)} \rightarrow \mathrm{H'+HF(v')}$, $\mathrm{H'+HF(v)} \rightarrow \mathrm{H+H'F(v')}$ and $\mathrm{H'+HF(v)} \rightarrow \mathrm{H_2(v')+F}$. To do so, for each value of the total angular momentum *J* we use Eqs.(3.33) and (3.34) to determine, from the parity-

adapted helicity-representation scattering (S) matrix $S^{J,P,p}_{\mathrm{v}jk,\mathrm{v}'j'k'}(E)$, the probability for inelastic relaxation from an initial state either into a particular HF(v′, j′) final state either with or without H atom exchange. In a similar way, we can determine the probability for reactive quenching.

From these transition probabilities, the intial- and final-state resolved integral cross section, summed over the final projection quantum number and averaged over the initial projection quantum number, is defined by

$$\sigma_{\mathrm{v},j\to\mathrm{v}',j'}(E_c) = \frac{\pi}{(2j+1)k_{\mathrm{v}jk}{}^2} \sum_{Jkk'} (2J+1) P^J_{\mathrm{v}jk,\mathrm{v}'j'k'}(E) \tag{3.35}$$

where vjk are the vibrational, rotational, and projection quantum numbers of the diatomic moiety (HF or H_2, depending on the channel), and J is the total angular momentum. The sum over J is truncated at a value $J_{\max}$ beyond which the reaction probability is negligible. Here, also, E is the total energy and E_c is the initial collision (translational) energy, with $E_c = E - \varepsilon_{\mathrm{v}jk}$. The quantity $k_{\mathrm{v}jk}$ is the initial wavevector, defined by $k_{\mathrm{v}jk}{}^2 = 2\mu E_c / \hbar^2$.

The overall integral removal cross section for a particular vibration-rotation level is obtained by summing Eq. (3.35) over all possible final states. We have

$$\begin{aligned} \sigma_{\mathrm{v}j}(E_c) &= \sum_{\mathrm{v}'j'} \sigma_{\mathrm{v}j\to\mathrm{v}'j'}(E_c) \\ &= \frac{\pi}{(2j+1)k_{\mathrm{v}jk}{}^2} \sum_{Jkk'\mathrm{v}'j'} (2J+1) \left| S^J_{\mathrm{v}jk,\mathrm{v}'j'k'}(E) \right|^2 . \end{aligned} \tag{3.36}$$

Alternatively, by limiting the sum over final states in Eq. (3.36), one can determine the vibrational removal cross section associated with the direct and exchange inelastic processes as well as with reactive quenching.

As shown, schematically, in Fig. 3.3, other relevant quantities such as cumulative reaction probabilities $N_{\mathrm{v}}^{J}(E)$, detailed state-to-state rate constants $k_{\mathrm{v},j\to\mathrm{v}',j'}(T)$ and overall vibrational relaxation rate constant $k_{\mathrm{v}}(T)$ can be obtained from the fundamental *S* matrix. These quantities will be introduced and defined in the following subsection.

3.4.2. State-to-State Rate Constants and Vibrational Relaxation Rate Constants

Let us imagine a collision event involving atom A and molecule BC. Let the relative velocity be *u*. If the concentration of A is $[A]$, the flux of atoms A impinging on BC is given by $I_A = u[A]$. The infinitesimal change in intensity of the initial beam of atoms A due to scattering by BC after passing through a distance *dl* is

$$dI_A = -\sigma(u) I_A(l)[BC]dl \tag{3.37}$$

Here $\sigma(u)$ is the integral scattering cross section, which is the function of the incident translational energy (or, alternatively, of the velocity *u*). Since $I_A = u[A]$ and $u = dl/dt$

$$-(d[A]/dt) = u\sigma(u)[A][BC] \tag{3.38}$$

In general, for a binary collision process, the second-order rate equation is given by

$$-d[A]/dt = k(T,u)[A][BC] \tag{3.39}$$

where $k(u)$ is the velocity-resolved rate constant. Comparing Eqs. 3.38 and 3.39, we see that $k(u)$ is just the integral cross section multiplied by the A–BC relative velocity.

If we have a Maxwellian distribution of relative velocities, then the thermal rate constant $k(T)$ is obtained by velocity averaging, namely[30]

$$k(T) = < u\sigma(u) > = 4\pi(\mu / 2\pi k_B T)^{3/2} \int_0^\infty u^3 \sigma(u) \exp(-\mu u^2 / 2k_B T) du \tag{3.40}$$

where k_B is Bolzmann's constant.

Consider the state-resolved process $\mathrm{A+BC(v}, j) \rightarrow \mathrm{C+AB(v'}, j')$. For this process, the corresponding rate constant is $k_{\mathrm{v},j \rightarrow \mathrm{v}',j'}(T)$ and the corresponding rate equation is[31]

$$-\frac{d[BC(\mathrm{v}, j)]}{dt} = \frac{d[AB(\mathrm{v}', j')]}{dt} = k_{\mathrm{v},j \rightarrow \mathrm{v}',j'}(T)[A][BC(\mathrm{v}, j)] \tag{3.41}$$

The rate equation for the overall vibrational relaxation of the chemical species $BC(\mathrm{v})$ can be expressed as

$$-\frac{d[BC(\mathrm{v})]}{dt} = \sum_{\mathrm{v}'jj'} k_{\mathrm{v},j \rightarrow \mathrm{v}',j'}(T)[A][BC(\mathrm{v}, j)] \tag{3.42}$$

If we assume the rotational levels of the reactant are in thermal equilibrium at temperature T, then

$$\frac{[BC(\mathrm{v}, j)]}{[BC(\mathrm{v})]} = \frac{[BC(\mathrm{v}, j)]}{\sum_j [BC(\mathrm{v}, j)]} = f_j(T) \tag{3.43}$$

$$f_j(T) = \frac{g_j \exp(-E_{\mathrm{v}j} / kT)}{\sum_j g_j \exp(-E_{\mathrm{v}j} / kT)} = \frac{g_j \exp(-E_{\mathrm{v}j} / kT)}{Q_{rot}(T)} \tag{3.44}$$

where $g_j = 2j+1$ is the degeneracy factor and Q_{rot} is the rotational partition function of a heteronuclear diatomic molecule. Substituting $[BC(\mathrm{v}, j)]$ in Eq. (3.42) we obtain

$$-\frac{d[BC(\mathrm{v})]}{dt} = \sum_{\mathrm{v}'jj'} k_{\mathrm{v},j\to\mathrm{v}',j'}(T)[A][BC(\mathrm{v})]f_j(T) = k_{\mathrm{v}}(T)[A][BC(\mathrm{v})] \tag{3.45}$$

$$k_{\mathrm{v}}(T) = \sum_j f_j k_{\mathrm{v},j}(T) = \sum_j f_j \sum_{\mathrm{v}'j'} k_{v,j\to\mathrm{v}',j'}(T) \tag{3.46}$$

Thus, the vibrational relaxation rate constant $k_{\mathrm{v}}(T)$ can be calculated by summing the state-to-state rate constant $k_{\mathrm{v},j\to\mathrm{v}',j'}(T)$ over final vib-rotational states $\mathrm{v}'j'$ then averaging over initial rotational states j. The relationship between the integral cross section and the thermal vibrational relaxation rate constants is

$$k_{\mathrm{v}}(T) = \sum_j f_j \sum_{\mathrm{v}'j'} 4\pi(\mu/2\pi k_B T)^{3/2} \int_0^\infty u^3 \sigma_{\mathrm{v},j\to\mathrm{v}',j'}(u)\exp(-\mu u^2/2k_B T)du \tag{3.47}$$

Substituting f_j by using Eq. (3.44) and integrating over the collision energy $E_C = \frac{1}{2}\mu u^2$, we obtain

$$k_{\mathrm{v}}(T) = (\frac{1}{\pi\mu})^{\frac{1}{2}}(\frac{2}{k_B T})^{\frac{3}{2}}\frac{1}{Q_{rot}}\int_0^\infty E_C e^{-\frac{E_C}{k_B T}}\sum_j g_j \sum_{\mathrm{v}'j'}\sigma_{\mathrm{v},j\to\mathrm{v}',j'}(E_C)e^{-\frac{E_{\mathrm{v}j}}{k_B T}}dE_C \tag{3.48}$$

where $E_C = \frac{h^2 k_{\mathrm{v}j}^{\ 2}}{8\pi^2\mu} = E - E_{\mathrm{v}j}$ is the translational energy of the system. If we change the integration variable to the total energy E of the system, this equation becomes[31]

$$k_{\mathrm{v}}(T) = \frac{1}{(2\pi\mu k_B T/h^2)^{3/2}Q_{rot}}\int_0^\infty \sum_j g_j h^{-1}\frac{k_{\mathrm{v}j}^{\ 2}}{\pi}\sum_{\mathrm{v}'j'}\sigma_{\mathrm{v},j\to\mathrm{v}',j'}(E)e^{-\frac{E}{k_B T}}dE \tag{3.49}$$

We can write this equation as

$$k_{\mathrm{v}}(T) = \frac{1}{Q_{trans}(T)Q_{rot}(T)}\int_0^\infty h^{-1}\mathbb{Z}_{\mathrm{v}}(E)e^{-\frac{E}{kT}}dE = \frac{P(T)}{Q(T)} \tag{3.50}$$

with

$$\mathbb{Z}_{\mathrm{v}}(E) = \sum_{j} g_j \frac{k_{\mathrm{v}j}{}^2}{\pi} \sum_{\mathrm{v}'j'} \sigma_{v,j\to \mathrm{v}',j'}(E) \tag{3.51}$$

where $Q_{trans}(T) = (2\pi\mu kT/h^2)^{3/2}$ is the translation partition function for an ideal gas at temperature T.

By using Eq. 3.35, the function $\mathbb{Z}_{\mathrm{v}}(E)$ can be expressed in terms of the collision *S*-matrix elements

$$\begin{aligned} \mathbb{Z}_{\mathrm{v}}(E) &= \sum_{j} (2j+1) \frac{k_{\mathrm{v}j}{}^2}{\pi} \sum_{\mathrm{v}'j'} \sigma_{\mathrm{v}j\to \mathrm{v}'j'}(E) \\ &= \sum_{Jkk'jj'\mathrm{v}'} (2J+1) \left| S^{J}_{\mathrm{v}jk,\mathrm{v}'j'k'}(E) \right|^2 = \sum_{J} (2J+1) N^{J}_{\mathrm{v}}(E) \end{aligned} \tag{3.52}$$

Finally, it is easy to show that the vibrational relaxation rate constant can be written as the weighted average of the state-to-state rate constants

$$k_{\mathrm{v}}(T) = \frac{\sum_{j} g_j e^{-\frac{E_{\mathrm{v}j}}{k_B T}} \sum_{\mathrm{v}'j'} k_{\mathrm{v},j\to \mathrm{v}',j'}(T)}{Q_{rot}(T)} \tag{3.53}$$

Fig. 3.3 shows a flow chart that summarizes the computational procedure outlined in this chapter. Again, $S^{J,P,p}_{\mathrm{v}jk,\mathrm{v}'j'k'}$ designates an element of the parity-adapted *S* matrix, which is the output from our scattering calculation. More advanced observables such as state-to-state cross sections $\sigma_{\mathrm{v},j\to \mathrm{v}',j'}(E_C)$, overall cross sections $\sigma_{\mathrm{v},j}(E_C)$, detailed state-to-state rate constants $k_{\mathrm{v},j\to \mathrm{v}',j'}(T)$ and vibrational relaxation rate constants $k_{\mathrm{v}}(T)$ can be obtained from the S matrix for all relevant channels. The next chapter will present the results of our calculations for the vibrational relaxation of HF(v) in collisions with H atoms .

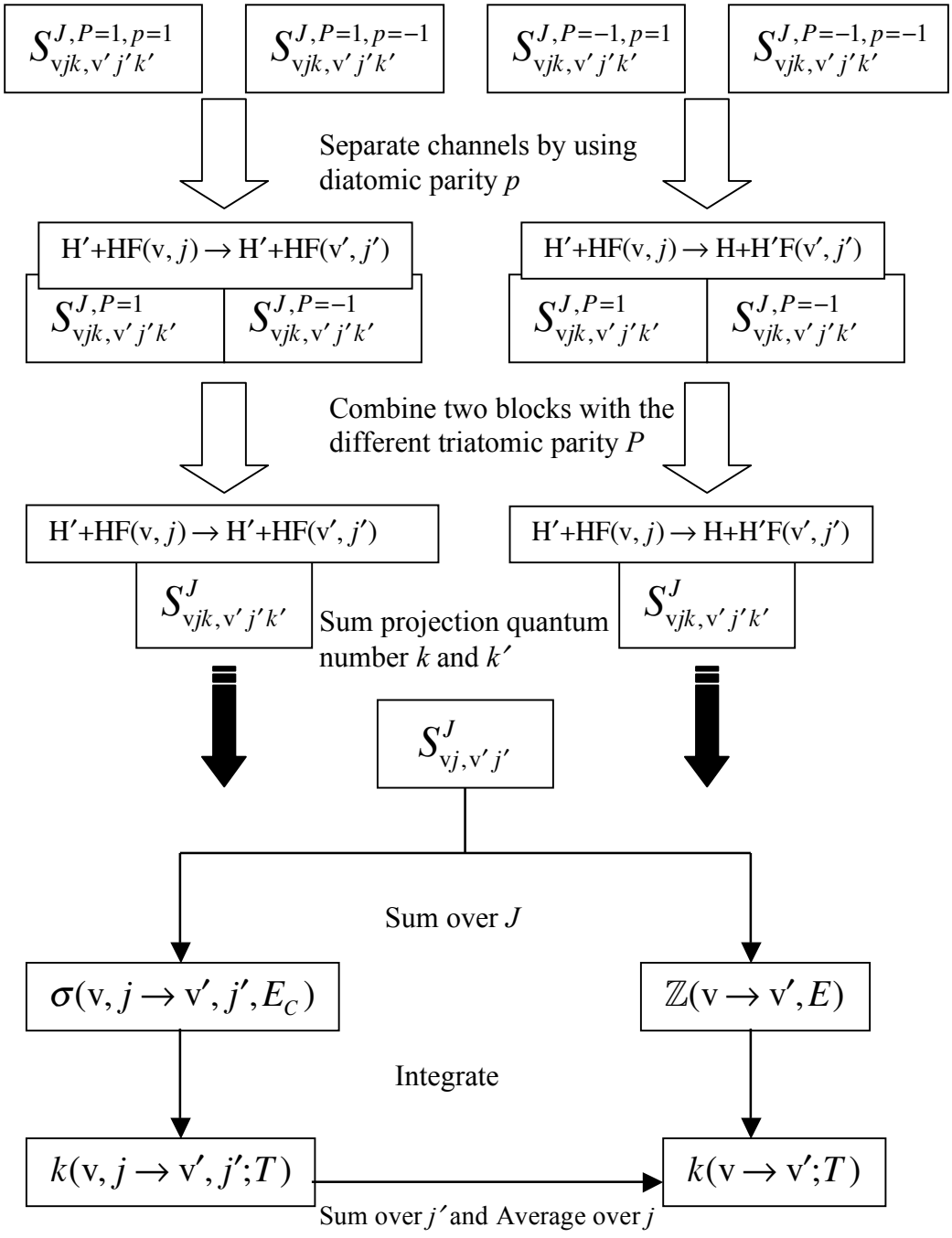

Figure 3.3 Calculation flow chart. Here S denotes the scattering matrix output from the ABC code; σ is the integral cross section and k is the rate constant

Chapter 4: Results and Discussions

4.1 Scattering calculations

As far as we are aware, the work described here is the first application of quantum reactive scattering methodology to the study of inelastic HF scattering in collision with H atoms. Therefore, to ensure the accuracy of our results, we carried out extensive convergence tests with respect to increasing the size of the rotational-vibrational basis and the number of propagation sectors. As we have stated earlier in Chapter 3, in the ABC code, the size of the channel basis is defined by three parameters: e_{max}, j_{max} and k_{max}. All HF (or H_2) vibration-rotation states with rotational angular momentum less than or equal to j_{max}, and, simultaneously, energy less than e_{max} are included. In addition, only projection states with $k \leq k_{max}$ are included.

For a defined vibration-rotation-projection basis, the precision of the scattering calculations is defined by two parameters: r_{max}, which defines the maximum interparticle distance (technically, the maximum hyperradius) beyond which the potential is assumed to vanish, and n_{max} , which sets the number of numerical integration sectors. In addition, the precision of the calculated integral cross sections depends on the parameter J_{max} which defines the maximum partial wave included. For total angular momenta larger than *J,* the centrifugal barrier is so

large that the collision partners never penetrate close enough for the inelastic coupling to be effective.

Table 4.1 lists the values of these parameters that we have used in our scattering calculations on the SW-PES. In general, the higher the total energy, the larger the basis set required. For relaxation of HF(v) at a given collision energy, the higher the value of v, the greater the total energy. Thus to determine cross sections for the higher vibrational levels of HF required, for convergence, larger basis sets – and, consequently, longer computation times.

Table 4.1 Summary of parameters used in our scattering calculations on SW-PES

	J	e_{max}	j_{max}	k_{max}	r_{max}	n_{max}
v=5	0-26	2.775	27	4	11	500
v=4	0-24	2.825	26	4	12	550
v=3	0-21	2.700	24	4	12	500
v=2	0-20	2.1	20	3	14	500

4.2 Comparison of the three channels for vibrational relaxation of HF(v=3)

Figure 4.1 displays the integral cross sections for vibrational relaxation of HF(v=3, j=0) as a function of the collision energy. Cross sections for each of the three channels (direct inelastic, exchange inelastic and reactive quenching) have been

labeled. At energies below 0.031eV, which is the difference between the lowest bent barrier and the HF(v=3, *j*=0) asymptote, there appear strong oscillations and narrow peaks in the integral cross sections. As we will discuss later in this thesis (Chapter 5), this structure is a manifestation of scattering resonances which arise because of the weak HF–H attractive van der Waals interaction.

We observe in Fig. 4.1 that the direct inelastic process dominates at low energy. As the energy increases, reactive quenching becomes more important and eventually dominates. This can likely be explained on energy gap arguments. The HF(v=3, *j*=0) level lies 0.035 eV above the H_2(v=0, *j*=0) level. However the HF(v=2, *j*=0) level lies 0.45 eV below the HF(v=3, *j*=0) level. In a simplistic model, the efficiency of reactive as compared to inelastic quenching will depend first on the energy gap between the initial and the two final states. In general, the smaller the energy gap, the more efficient the energy transfer. Also, however, for a given energy gap, statistical arguments, based on the volume of available phase space, suggest that the larger the translational energy in the particular final state, the greater will be the cross section.[31]

Although the energy gap is much smaller for the HF(v=3, *j*=0)+H→H_2(v=0, *j*=0)+F channel, the product translational energy will be much larger for the HF(v=3, *j*=0)+H→ HF(v=2, *j*=0)+H channel. Consequently, at low collision energy, where the difference in product translation energy is largest, the inelastic channel will dominate. At higher collision energies, however, the reactive channel becomes increasingly important.

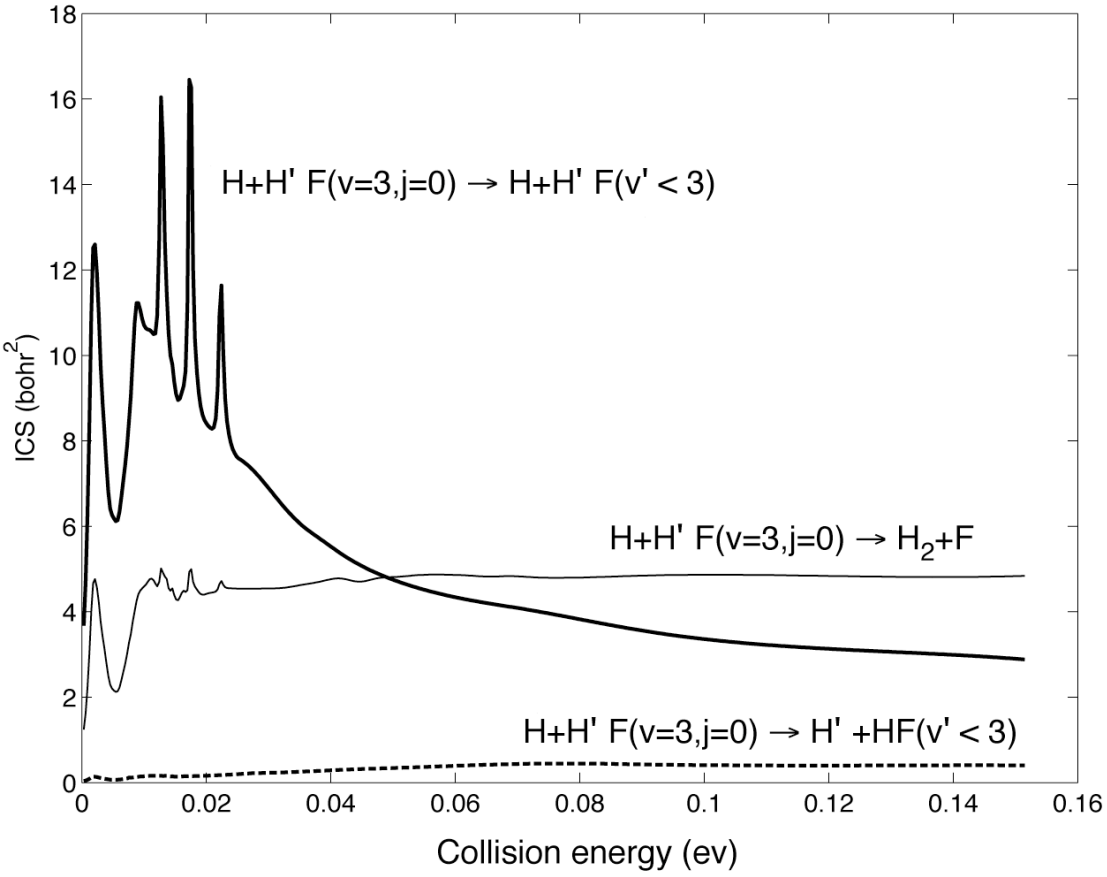

Figure 4.1 Plot of the integral cross sections (ICS) for vibrational relaxation of HF(v=3, *j*=0) as a function of the collision energy. Cross sections for each of the three channels (direct inelastic, exchange inelastic and reactive quenching) have been shown.

4.3 Comparison of direct inelastic and exchange inelastic cross sections

Fig. 4.2 shows the integral cross section for the two inelastic processes: direct and exchange, as a function of the initial HF vibrational quantum number v. We find that inelastic collisions with atom exchange are much less efficient at relaxing vibrationally excited HF. This is surely a result of the high barrier to atom exchange.

As shown in Table 2.2, on the SW potential energy surface the H–F–H barrier lies 0.31 eV (7.15 kcal/mol) above the HF(v=3, *j*=0)+H asymptote, but 0.12 eV (2.79 kcal/mol) below the HF(v=4, *j*=0)+H asymptote.

For HF in v=3, 4 and 5 with *j* =0, inelastic collisions with atom exchange are not as efficient a process for vibrational relaxation as either the direct inelastic or reaction mechanisms. For the direct inelastic processes, and as is typical for many other inelastic processes, the cross sections rise steeply with increasing collision energy. Vibrational relaxation is the result of distortion of the HF potential by approach of the H atom. At very low collision energy, the basically repulsive HF–H interaction prevents the collision partners from approaching close enough to sample forces strong enough to result in significant vibrational inelasticity. This effect may be compounded by the presence of a small, artificial barrier at long range in the SW potential energy surface due to an artifact in the fitting of the *ab initio* points. We will discuss this small barrier in more detail in Chapter 5.

As the energy increases, the inelastic cross sections rise and then fall at still higher collision energy. As the energy increases, it is likely that rotational excitation within the HF(v) manifold takes away some flux from the vibrational relaxation process. Consequently, as seen in Fig. 4.2, the vibrational relaxation cross sections drop slightly.

We also observe in Figs. 4.2 and 4.3 a large amount of structure in the energy dependence of the cross sections for relaxation out of HF(v=3) and, to a lesser extent, out of HF(v=2). As we will discuss in Chap. 5 below, this structure corresponds to

scattering resonances due to the weak, long-range HF–H attractive van der Waals interaction.

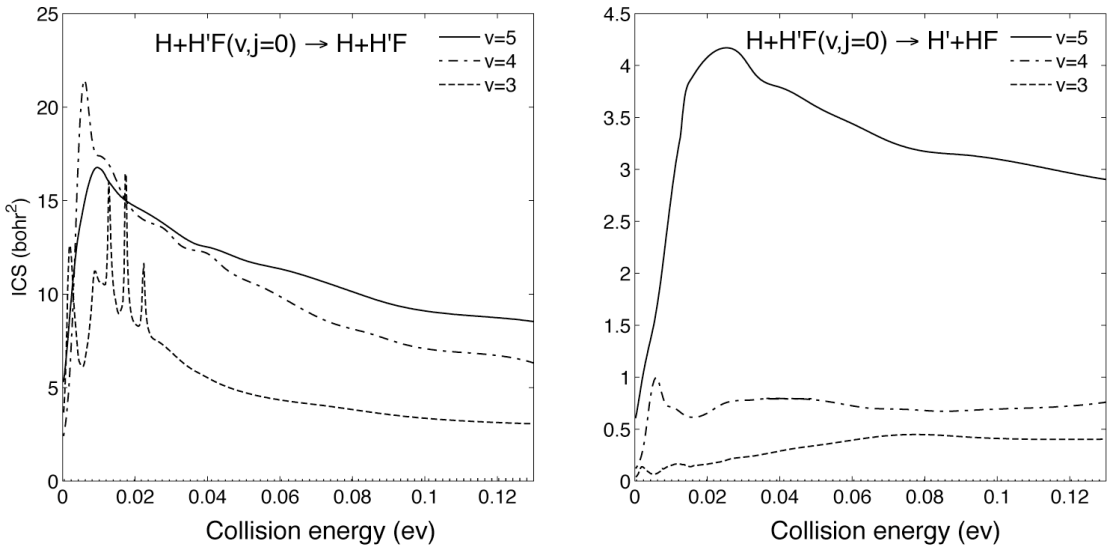

Figure 4.2 Plots of the integral cross section for the direct inelastic (left panel) and exchange inelastic (right panel) processes as a function of the initial HF vibrational quantum number v. The v=2 cross sections are too small to be distinguishable on these plots.

4.4 Comparison of multi-quantum transitions and single-quantum transitions

Figure 4.3 displays the integral cross sections for removal into particular vibrational final states with $v' < v$. As can be seen, in all cases the single vibrational quantum ($\Delta v = -1$) transitions dominate. This is particularly true for v=3 and 2. This is predicted by the simplistic early theory developed by Schwartz, Slawsky, and

Herzfeld (SSH theory),[32] which is based on the application of first-order perturbation theory and the assumption of simple, exponentially-repulsive vibrational coupling.

We see that the lower the degree of initial HF vibrational excitation, the more dominant becomes the single quantum ($\Delta v = -1$) process. At high collision energies, it appears (at least for v=5 and 4) that the direct correlation of the magnitudes of the integral cross sections with increasing Δv begins to break down.

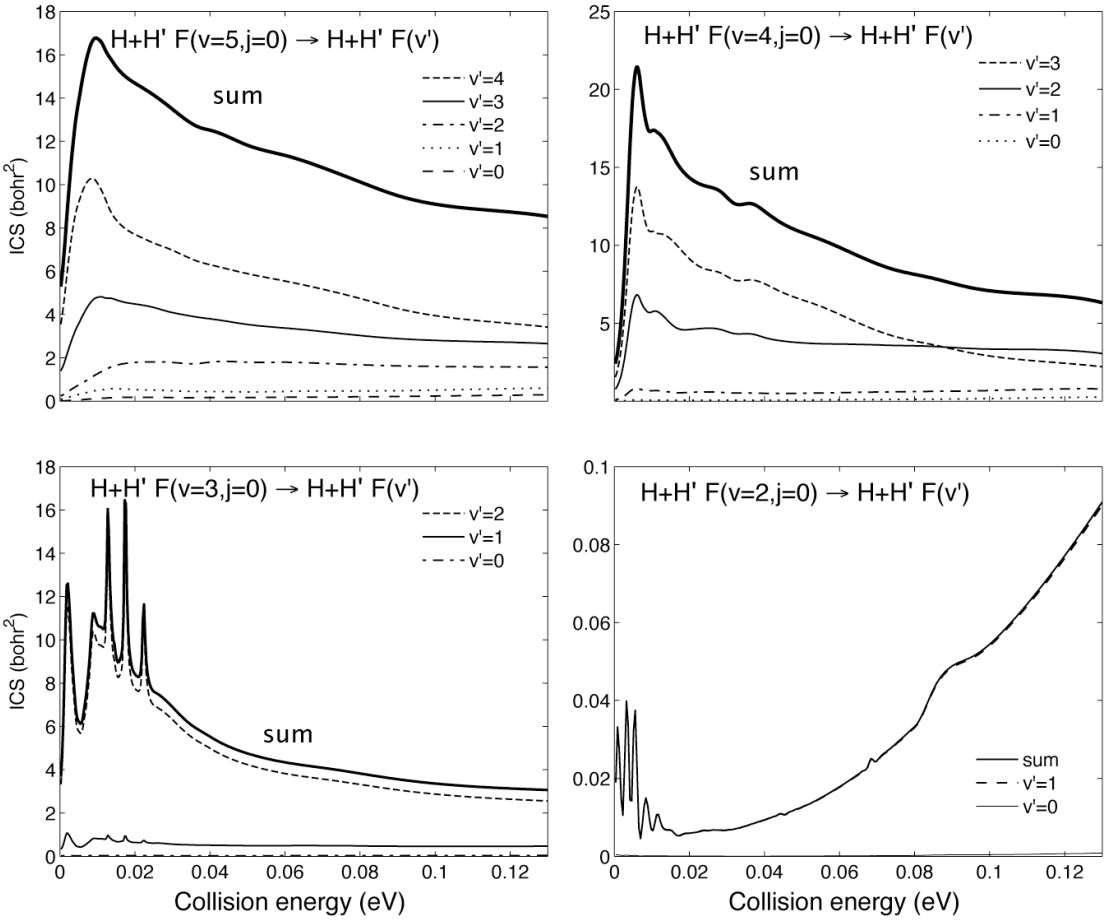

Figure 4.3 Plots of integral cross sections for direct inelastic $H+H'F(v, j=0) \rightarrow H+H'F(v' < v)$ removal into particular final vibrational manifolds, summed over final rotational quantum number.

4.5 Final rotational state populations

For the dominant direct inelastic process, Figs. 4.4 and 4.5 show the dependence of the final-state-resolved vibrational relaxation cross sections as a function of the final rotational quantum number at several values of the collision energy for the v=3→2 and v=3→1 transitions. The cross sections at low (0.0143 eV), intermediate (0.0515 eV) and higher (0.0915 eV) collision energies display a similar pattern. In every case the vibrational relaxation is accompanied by a modest degree of rotational excitation, with a maximum at $j' \cong 5$. The HF rotational constant is ~ 20 cm^{-1}, so that the rotational energy for $j = 5$ is $\cong 0.1$ eV. Since the vibrational spacing in HF is $\cong 0.5$ eV, we see that most of the energy is lost into translation, particularly for the Δv=2 transitions. Consequently, Fig. 4.4 confirms the conclusion, mentioned in Chapter 1, of the early quasi-classical trajectory calculations[8] that the main inelastic (HF+H) energy transfer process involves vibrational energy conversion into translational energy and the minor energy transfer process is for vibrational energy to be converted into rotational energy.

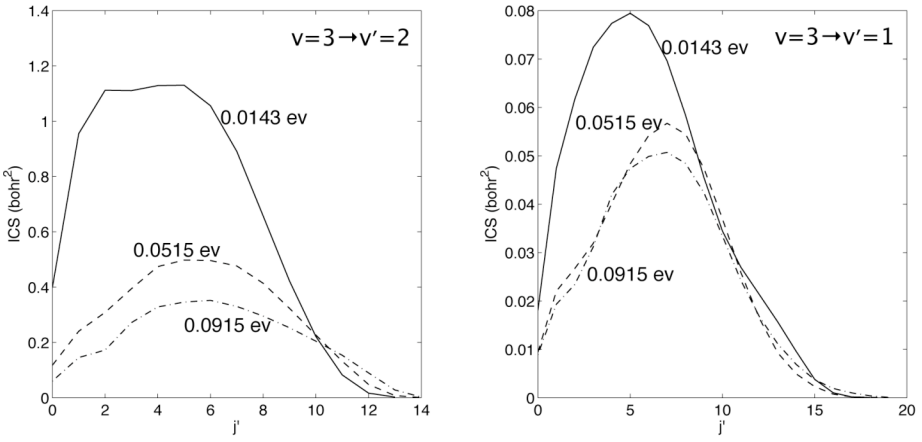

Figure 4.4 Plots of the integral cross sections (ICS) to specific final rotational states j' at collision energies of 0.0143 eV, 0.0515 eV and 0.0915 eV for the v=3→2 and v=3→1 transitions

4.6 Removal rate constants and cumulative reaction probabilities

We recall from Chap. 3 that the vibrational relaxation rate constant can be expressed as

$$k(\mathrm{v};T) = \frac{1}{Q_{trans}(T)Q_{rot}(T)} h^{-1} \int_0^\infty \mathbb{Z}_{\mathrm{v}}(E) \exp\left(-E/kT\right) dE \qquad (4.1)$$

where $Q_{trans}(T)$ is the translation partition function for an ideal gas at temperature T, and Q_{rot} is the rotational partition function of the HF molecule. The function $\mathbb{Z}_{\mathrm{v}}(E)$ is

$$\mathbb{Z}_{\mathrm{v}}(E) = \sum_{j}(2j+1)\frac{{k_{\mathrm{v}jk}}^2}{\pi}\sum_{\mathrm{v}'j'}\sigma_{\mathrm{v}j\to\mathrm{v}'j'}(E)$$
$$= \sum_{JPpkk'jj'\mathrm{v}'}(2J+1)\left|S^{JPp}_{\mathrm{v}jk,\mathrm{v}'j'k'}(E)\right|^2 = \sum_{J}(2J+1)N^{J}_{\mathrm{v}}(E) \qquad (4.2)$$

Here $N^{J}_{\mathrm{v}}(E)$ is called the cumulative reaction probability[33] at total energy E, and is defined by

$$N^{J}_{\mathrm{v}}(E) = \sum_{Ppkk'jj'\mathrm{v}'}\left|S^{JPp}_{\mathrm{v}jk,\mathrm{v}'j'k'}(E)\right|^2 \qquad (4.3)$$

Fig. 4.5 plots the calculated cumulative reaction probabilities for the three H+H′F(v=3) removal channels. We see, clearly here, two pronounced peaks (marked "A" and "C" on the figure) and a less distinct feature in between (marked "B" on the figure). For total angular momentum J=0, all of these peaks occur above the threshold (E_{tot} = 0.3035 eV) for the H+H′F(v=3) reaction. As will be discussed in Chapter 5 of this thesis, these peaks correspond to enhancement of the overall vibrational removal cross section due to effect of quasi-bound resonances in the HF–H valley.

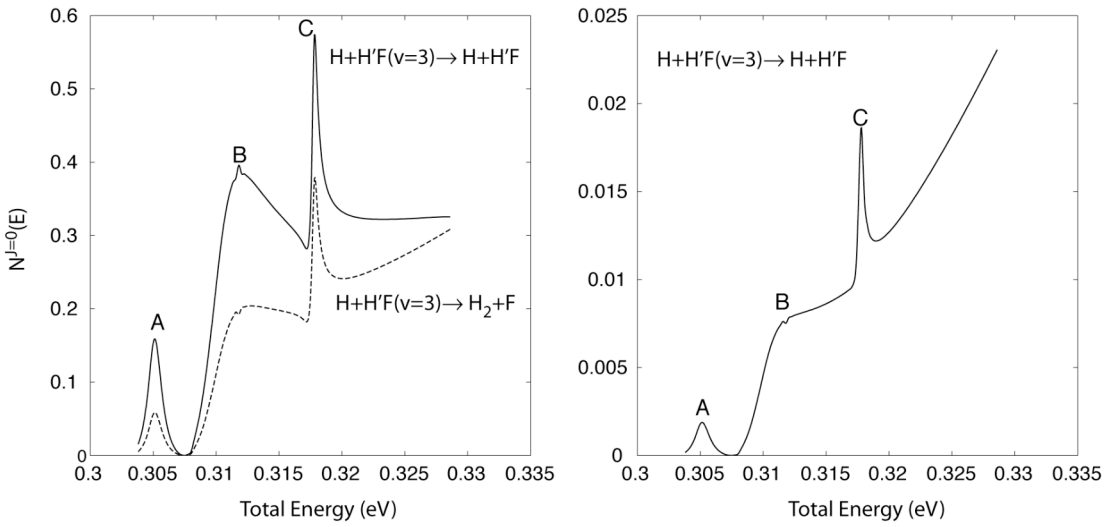

Figure 4.5 Plots of the calculated cumulative reaction probabilities for the three H+H′F(v=3) removal channels as a function of total energy. Total angular momentum J=0

From Eq. (3.40) we see that the thermal rate constant is an average over a Maxwellian velocity distribution of the product of the relative velocity times the cross section. Thus, we can define a "thermal cross section" as

$$\sigma = k(T) / u(T) \tag{4.4}$$

where *u(T)* is the average speed

$$u(T) = \left[\frac{8kT}{\pi\mu} \right]^{1/2} \tag{4.5}$$

with μ being the HF–H reduced mass. If we introduce the experimental or QCT rates into Eq. (4.4), we obtain the thermal cross sections shown in Tables 4.2 and 4.3. From Eq. (4.5) the average collision energy is $\frac{1}{2}\mu u(T)^2 = 4kT / \pi$. At T=295 K this is 0.03 eV. Tables 4.2 and 4.3 also show the corresponding integral cross section for vibrational relaxation of H+H′F(v=3, j=0) from our quantum scattering calculations at

this energy. We observe considerably better agreement with the earlier experiments than in the case of the QCT calculations.

Table 4.2 Thermal (T=295K) cross sections (bohr^2) for vibrational deactivation of HF(v=3) by H atoms.

	Total	Channel (1c)	Channel (1a)+(1b)
Experimental measurements	14.6	3.3	11.3
QCT calculations	4.9	0.95	4.0
Quantum scattering calculations	12.8	4.8	8.0

Table 4.3 Thermal (T=295K) cross sections (bohr^2) for vibrational deactivation of HF(v=2) by H atoms.

	Total	Channel (1c)	Channel (1a)+(1b)
Experimental measurements	0.15	… [a]	0.15
QCT calculations	2.2	… [a]	2.2
Quantum scattering calculations	0.01	… [a]	0.01

a. The HF(v=2)+H→H_2+F reaction is energetically inaccessible.

We observe from a comparison of these two tables with Figs. (4.2) and (4.3) that the present fully-quantum scattering calculations on the *ab initio* Stark-Werner

potential energy surface yield vibrational removal cross sections which agree to better than an order of magnitude with the earlier experimental results and the results of QCT calculations based on a far cruder potential energy surface.

4.7 Discussion and conclusion

Our calculations predict substantial cross sections for vibrational relaxation of HF in collisions with H atoms. By taking suitable linear combinations of the definite-parity *S*-matrix elements, we can resolve cross sections for the inelastic [HF(v)+H→HF(v′<v)+H] relaxation pathway into the contributions due to direct inelastic scattering without H atom exchange and the contributions due to inelastic scattering accompanied by atom exchange. For all energies and for all vibrational levels considered, we find that the direct inelastic scattering is the dominant relaxation mechanism, followed, in order of decreasing importance, by reactive quenching [HF(v)+H→H_2+F], and by inelastic scattering due to atom exchange.

The inefficiency of the latter process can be explained, in part, by the high energetic barrier to F atom exchange. However, even for HF(v=5), which lies well above the barrier, we see in Fig. 4.2 that the cross sections for the atom exchange mechanism are only ~ 20% of those for direct inelastic relaxation.

It is worthwhile to compare these cross sections with those for the relaxation of OH by collisions with H atoms, studied a few years ago in our research group by Atahan.[34] This is a very different system. The deep H_2O well provides a mechanism for complex formation, in which initial OH vibrational energy can be efficiently

redistributed. Figure 4.6 shows, for reference, the vibrational removal cross sections determined by Atahan and Alexander. The sharp increase in the cross sections at low collision energy is characteristic of a process involving transient complex formation, and so is very different from the low-energy behavior of the removal cross sections we calculate for the HF(v)+H system. Nevertheless, except at the lowest energies, the magnitudes of the OH vibrational removal cross sections are on the order of 10 bohr^2, which is not too much larger than we predict for the vibrational removal cross sections of FH, where there is no deep attractive well.

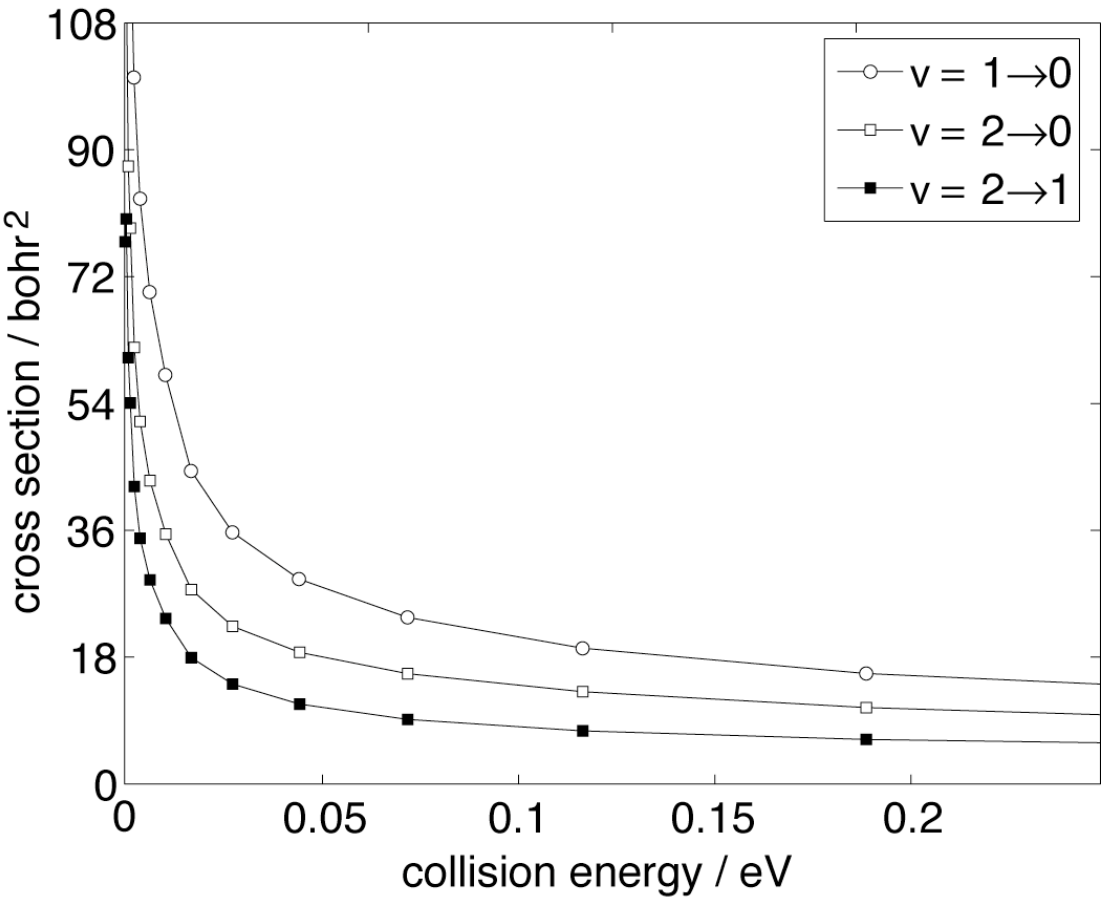

Figure 4.6 Initial state selected vibrational removal cross sections for OH(v) in its lowest rotational level in collisions with H atoms. Adapted from Fig. 7 of Ref. 33.

In the investigation by Atahan, a statistical close-coupled model was used.[35] Within this model, because the OH+H′ and OH′+H arrangements are not directly linked, it is impossible to distinguish between energy transfer with, or without, atom exchange. Also, the $O(^1D)+H_2$ channel, which could, in principle, correspond to a reactive quenching process, is energetically inaccessible.

By contrast, recently Krems, Nordholm, and co-workers described close-coupled calculations of vibrational relaxation cross sections for collisions of HF(v=1) with the closed-shell Ar atom.[36] The computed cross sections are less than 10^{-3} $bohr^2$ for collision energies below ~ 0.25 eV. This is far lower than the H+HF vibrational removal cross sections we have calculated here. It is the distortion of the diatomic vibrational potential, engendered by approach of the atomic target, which is responsible for vibrational relaxation. Clearly, then, the distortion of the HF potential produced by approach of H is much stronger than by approach of Ar. This is because, even for energies below the H–F–H barrier, the HF bond is substantially weakened by incipient atom exchange.

We observed the presence of numerous narrow peaks in the energy dependence of both the integral cross section and cumulative reaction probabilities for vibrational relaxation of HF(v=3). As will be investigated in more detail in Chapter 5, these sharp peaks are evidence of the role of resonances, which reflect trapping in the weak HF–H van der Waals well. It can explain the reason why the QCT calculation underestimates the rate constant that has been measured by fluorescence experiment. Classical trajectories cannot account for tunneling and the

LEPs surface over estimates the height of reaction barrier for both exchange inelastic collision and reactive quenching. The comparison between the integral cross section for HF(v=3) and HF(v=2) (Figs. 4.2 and 4.3) indicates that the vibrational relaxation of HF(v=3) is approximately 100 times faster than the vibrational relaxation of HF(v=2). As the consequence of tunneling in quantum reactive scattering, this result matches the experimental measurements very well.

Chapter 5: The role of van der Waals resonance in the vibrational relaxation of HF in collisions with H atoms

5.1 Introduction

This work is motivated by our earlier study of the vibrational relaxation of HF(v) molecules by H atoms and by several previously groundbreaking investigations on the role of resonances in the reaction of F with H_2 and its isotopomers.[5,19,37-40] Here, the term "resonance"[41,42] refers to a transient metastable or quasi-bound state which is formed as the reaction occurs. The first case, sometimes called a "reactive resonance state",[38,39] is the result of a deep and thin trapping well located near the repulsive barrier (transition state) on the potential energy surface (PES). The second type of metastable state arises because of a shallow van der Waals well in the asymptotic region of a potential energy surface. A weakly bound "van der Waals state"[19,40] can act to slow down the motion of the system allowing a more efficient transfer of internal energy into the degree of freedom corresponding to motion over a reaction barrier.[42]

Due to the difficulty of carrying out molecular beam investigations with sufficient energy and angular resolution to observe scattering resonances, relatively few unambiguous observations have been reported. The observation of bimolecular

reactive scattering resonances have been confined to two fundamental reactions: $H+H_2$[43] , F+HD and F+ H_2.[41,44] From a theoretical point of view, in a bimolecular reaction a popular characterization of a resonance involves determination of the delay time associated with the relative motion of the colliding reactants. That is, at a collision energy corresponding to a resonance, the motion of the colliding reactants is poorly coupled to the reaction coordinate (minimum-energy path). However, if a "time delay" in the collision occurs, then the required energy redistribution can take place to surmount the reaction barrier. The time delay corresponds to persistence of a temporary quasi-bound state. Therefore, resonance peaks can be related to one or more metastable states along the reaction path, either at the transition state or in the product or reactant arrangements.

Our work on the role of resonances in HF(v)+H relaxation was inspired by the earlier work of Manolopoulos, Skodje and their coworkers on the appearance of resonance in the exothermic reaction of F with H_2 and HD.[19,38] In the latter case, the experimental signature of a resonance has been confirmed by Liu and coworkers.[41] This F+HD resonance had been investigated, theoretically, by means of several powerful tools, including time delay analysis,[39,45] the vibrationally adiabatic approximation approximation[19,46] and the spectral quantization method.[47]

As we have seen in Sec. 4.4, the overall vibrational removal cross sections for HF(v=3) show pronounced structure as a function of energy. In order to understand the position of these features, which we attribute to resonances, we shall use an adiabatic bender analysis,[48,49] similar to the analysis presented by Castillo *et al*.[19] in their investigation of differential cross sections for the F+ H_2 reaction. The position of

quasi-bound van der Waals states coincides precisely with the observed resonance energies. These calculations will, hopefully, provide motivation for future experimental search for resonance signatures in H+H′F quenching.

5.2 Scattering calculation

The investigation of the role of resonances in HF vibrational relaxation starts with the determination of integral cross sections for inelastic collisions of HF(v, j=0) in collision with H atoms. Here, we used an extremely fine grid of energies in order to map out completely the resonance features. A more complete discussion of the computational details has been given in Chapter 3 of this thesis.

Again, there are three distinct pathways for removal of vibrationally excited HF from v=3 state: (1) inelastic relaxation without atom exchange

$$HF(v, j)+H' \rightarrow HF(v'<v, j')+H' \quad , \tag{5.1}$$

(2) inelastic relaxation with atom exchange

$$HF(v, j)+H' \rightarrow H'F(v'<v, j')+H \quad , \tag{5.2}$$

and (3) chemical reaction

$$HF(v, j)+H' \rightarrow HH'+F \quad . \tag{5.3}$$

As discussed earlier in Chapter 3, by taking a suitable linear combination of the S-matrix elements associated with positive (p = 1) and negative (p = –1) interchange symmetry, it is possible to determine, separately, the cross sections associated with the direct and exchange inelastic channels [Eqs. (5.1) and (5.2)].

The overall integral removal cross section for a particular vibration-rotation level is obtained by summing Eq. (3.35) over all possible final states. We have

$$\sigma_{\mathrm{v}j}(E_c) = \sum_{\mathrm{v}'j'} \sigma_{\mathrm{v}j\to\mathrm{v}'j'}(E_c)$$
$$= \frac{\pi}{(2j+1)k_{\mathrm{v}jk}{}^2} \sum_{J\eta kk'\mathrm{v}'j'} (2J+1) \left| S^{J\eta}_{\mathrm{v}jk,\mathrm{v}'j'k'}(E) \right|^2 . \tag{5.4}$$

Alternatively, by limiting the sum over final states in Eq. (5.4), one can determine the vibrational removal cross section associated with the direct and exchange inelastic processes as well as with reaction [processes (1)–(3)].

Figs. 5.1 and 5.2 display the energy dependence of these integral removal cross sections for processes (1), (2), and (3), for an initial state of HF(v=3, *j*=0). We observe that inelastic vibrational relaxation without exchange is the dominant pathway, followed, in importance, by reactive quenching. Inelastic vibrational relaxation with exchange is relatively improbable, because the HF+H′→H′F+H barrier lies ~0.12 eV (2.74 kcal/mol) above the HF(v=3, *j*=0)+H asymptote.[50] Since this value significantly exceeds the range of collision energies sampled in Figs. 5.1 and 5.2, we conclude that over this range of collision energies inelastic vibrational relaxation with exchange occurs exclusively by quantum mechanical tunneling through the HF+H′→H′F+H barrier.

We observe in Figs. 5.1 and 5.2 that the energy dependence of the vibrational removal cross sections is not monotonic, but, rather, punctuated by four or five narrow peaks. As we shall demonstrate below, these peaks correspond to the position of quasibound states in the asymptotic HF–H valleys. Finally, we observe that the peaks occur, identically, in the energy dependence of the integral removal cross

sections for each of the three distinct removal mechanisms: inelastic relaxation with and without H-atom exchange and reaction. This confirms that the quasi-bound states of relevance are located in the HF–H valley, rather than in the F–H_2 valley, since the latter region of the potential energy surface is not accessed in the inelastic processes. In addition, since reactive quenching [process (3)] is exoergic by 0.0353 eV for HF(v=3), it is unlikely that weakly bound states in the F–H_2 valley will play a role.

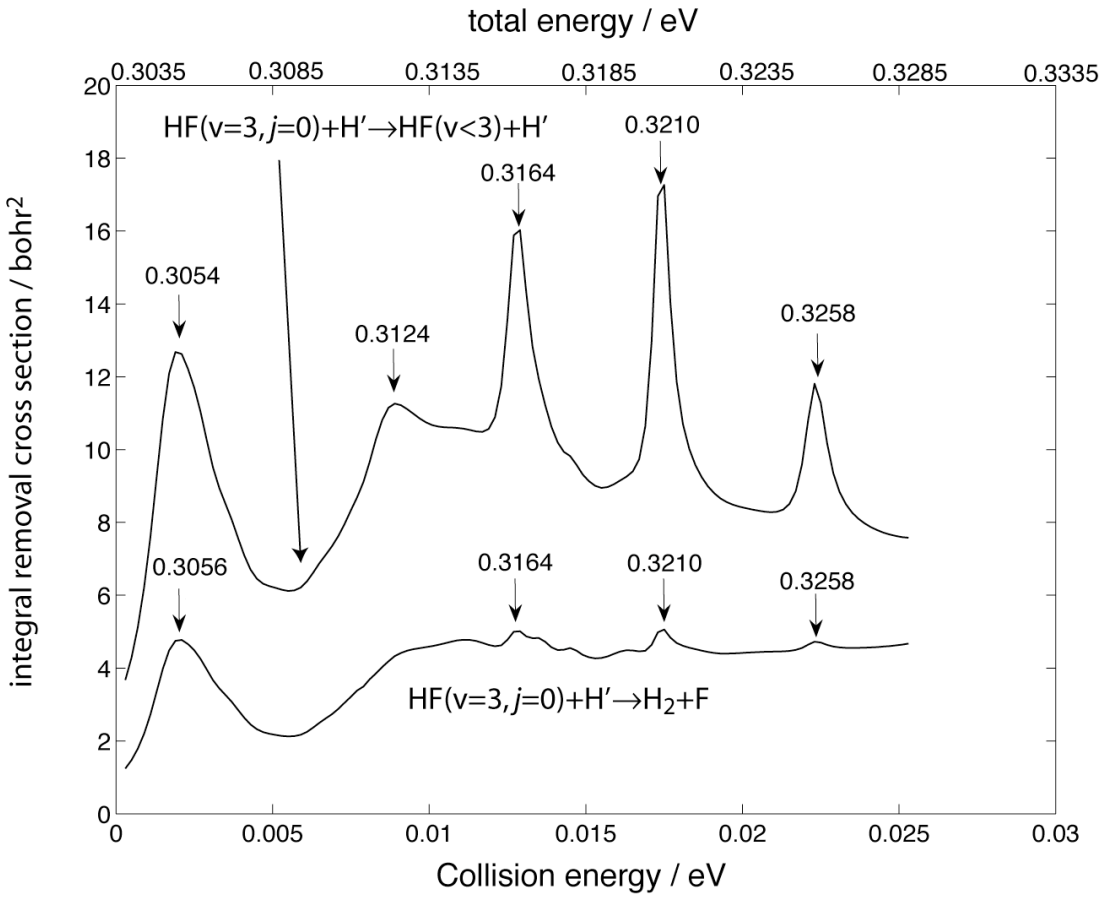

Figure 5.1 Dependence on collision energy of the HF(v=3, *j*=0) total removal cross section in bohr^2 for inelastic relaxation without atom exchange (top trace) and for reaction (lower trace). The HF(v=3, *j*=0) +H asymptote lies at 0.3035 eV above F+H_2 (r=r_e), which defines the zero of energy.

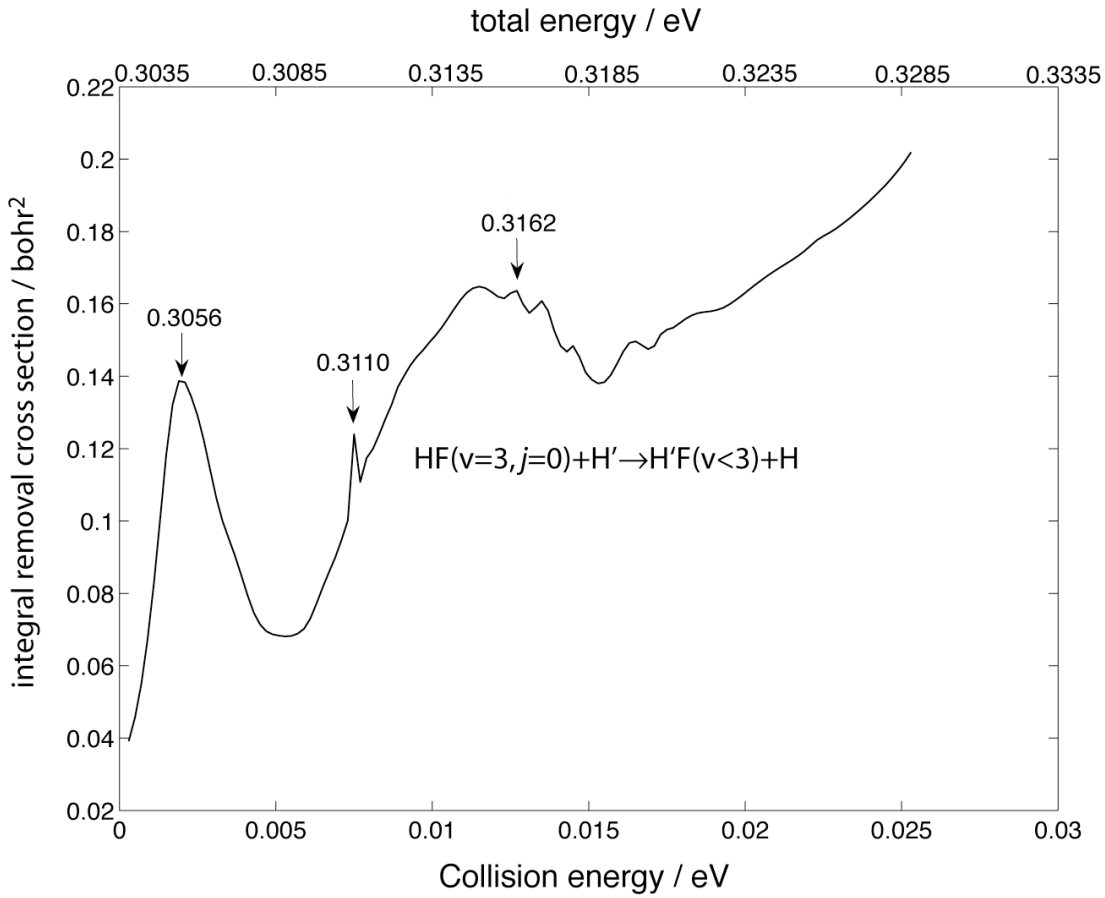

Figure 5.2 Dependence on collision energy of the HF(v=3, j=0) total removal cross section in bohr^2 for inelastic relaxation with atom exchange. The HF(v=3, j=0) +H asymptote lies at 0.3035 eV above F+H_2 (r=r_e), which defines zero of energy.

In Fig. 5.3 and 5.4 we show the contribution to the total removal probability for various individual values of the total angular momentum, again for the dominant direct inelastic process, namely

$$P_{vj}^{J} = (2J+1) \sum_{\eta kk'v'j'} \left| S^{J\eta}_{vjk,v'j'k'}(E) \right|^2 \quad . \tag{5.5}$$

Starting with J=0, each of these partial removal probabilities exhibits a prominent Lorentzian-like peak. The position of this peak shifts toward higher energy as J increases. It is clear that the lowest energy peak at E=0.3054 eV in the plot of the integral removal cross section in Fig. 5.1 arises from the overlap of the first peak in the low-J (J=0–4) partial removal probabilities. Also, the three narrow peaks in Fig. 5.1 at E=0.3164, 0.3210, and 0.3258 eV correspond to the peaks seen in Fig. 5.4 for the partial removal probabilities for J=10, 11 and 12.

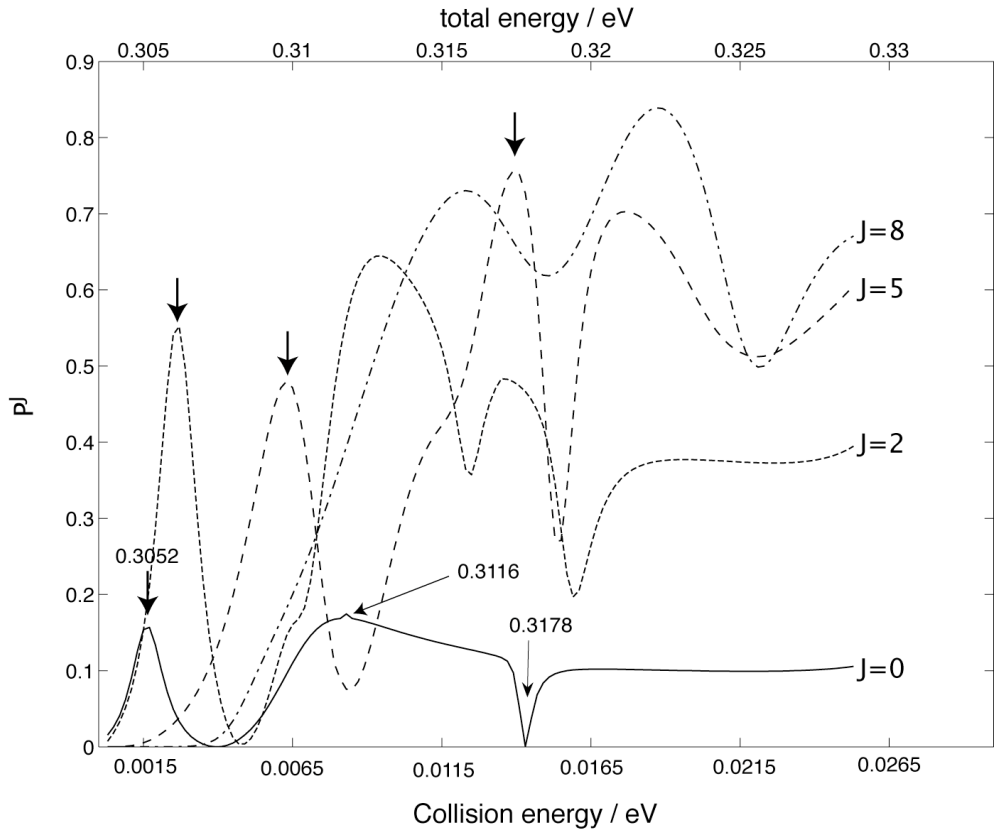

Figure. 5.3 Dependence on energy for the HF(v=3, *j*=0) partial removal probabilities [Eq. (5.5)] for values of the total angular momentum *J*=0, 2, 5, and 8. The heavy vertical arrows indicate the position of the *n*=1, *s*=1 adiabatic-bender quasi-bound states for *J*=0, 2, 5, and 8 (Table 5.1).

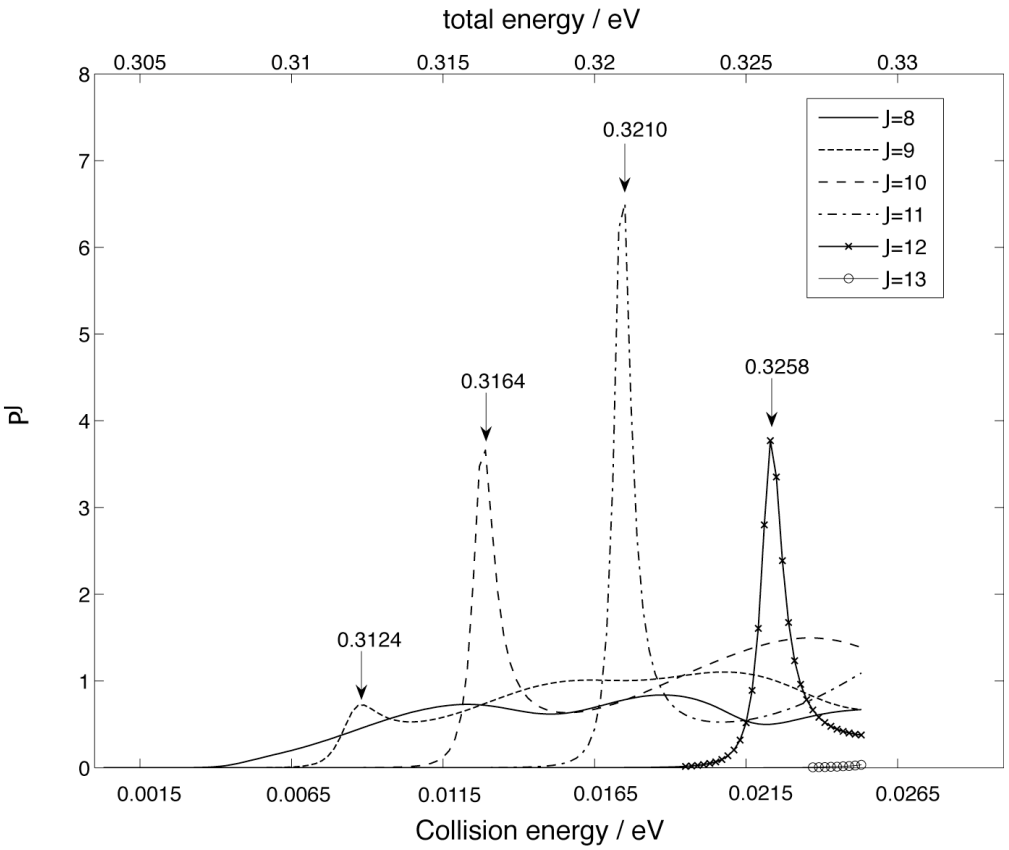

Figure. 5.4 Dependence on energy for the HF(v=3, *j*=0) partial removal probabilities [Eq. (5.5)] for values of the total angular momentum *J*=8–13. The vertical arrows indicate the position of the *n*=1, *s*=0 adiabatic-bender quasi-bound states for *J*=0, 2, 5, and 8 (Table 5.2).

In the next Section we shall use a simple adiabatic-bender model to explain the origin of the narrow resonance peaks observed in Figs (5.1)–(5.4).

5.3 Adiabatic bender model

In this section we shall use the adiabatic-bender model, first introduced by Holmgren, Waldman and Klemperer into the study of weakly-bound molecules,[48] to examine the origin of the sharp peaks seen in Figs. 5.1–5.4. A similar adiabatic model was used by Manolopoulos and co-workers[19] in the analysis of similar energy-dependent structure in $F+H_2 \rightarrow HF+H$ reactive cross sections. Grayce and Skodje have gone on to present a more extended adiabatic model[19,46] to analyze reactive resonances in heavy-light-heavy chemical reactions. We shall show that the resonance peaks observed in Figs. 5.1–5.4 can be associated with the quasi-bound states trapped in the van der Waals well in the HF–H arrangement.

The adiabatic-bender model starts first with an expansion of the scattering wavefunction in Jacobi coordinates appropriate to the HF–H product arrangement. In terms of these coordinates the Hamiltonian can be written as[23]

$$-\frac{\hbar^2}{2\mu_{H,HF}}\left(\frac{1}{R}\frac{\partial^2}{\partial R^2}R\right)-\frac{\hbar^2}{2\mu_{HF}}\left(\frac{1}{r}\frac{\partial^2}{\partial r^2}r\right)+\frac{\hat{l}^2}{2\mu_{H,HF}R^2}+\frac{\hat{j}^2}{2\mu_{HF}r^2}+V(R,r,\gamma) \quad (5.6)$$

Here $\vec{R}$ is the vector joining the H atom with the center-of-mass of the HF molecule, $\vec{r}$ is the HF bond axis, and γ is the angle between $\vec{R}$ and $\vec{r}$ [$\gamma = \cos^{-1}(\vec{R}\cdot\vec{r})$]. Also $\hat{l}$ and $\hat{j}$ are the operators represents the orbital angular momentum of the HF–H pair and the rotational angular momentum of the HF moiety, while μ_{HF} and $\mu_{H,HF}$ are the corresponding reduced masses.

$$\mu_{HF} = \frac{m_H m_F}{m_H + m_F} \quad (5.7a)$$

and

$$\mu_{\mathrm{H,HF}} = \frac{m_{\mathrm{H}}(m_{\mathrm{H}} + m_{\mathrm{F}})}{m_{\mathrm{H}} + m_{\mathrm{H}} + m_{\mathrm{H}}} \tag{5.7b}$$

We shall use a body-frame[26,28] development of the scattering wavefunction, identical to that used in the inelastic scattering of an atom by a molecule.[22,23] We first expand in terms of eigenfunctions of the total angular momentum and its projection, which are constants of the motion, namely

$$\Psi(\vec{R},\vec{r}) = \sum_{J=0}^{\infty} \sum_{M=-J}^{J} C_{JM} \Psi^{JM}(R,r,\gamma) \ . \tag{5.8}$$

We expand $\Psi^{JM}(R,r,\gamma)$ further as follows:[26]

$$\Psi^{JM}(R,r,\gamma) = \sum_{k=-J}^{J} D^{J*}_{Mk}(\phi,\theta,\psi) \Phi^{Jk}(R,r,\gamma) \sum_{j=|k|}^{\infty} \sum_{\mathrm{v}} \frac{1}{R} g^{Jk}_{\mathrm{v}j}(R) \left|\mathrm{v}jk\right\rangle \ , \tag{5.9}$$

where

$$\Phi^{Jk}(R,r,\gamma) = \sum_{j=|k|}^{\infty} \sum_{\mathrm{v}} \frac{1}{R} g^{Jk}_{\mathrm{v}j}(R) \left|\mathrm{v}jk\right\rangle \ . \tag{5.10}$$

Here, the angles ϕ, θ, and ψ describe the orientation of the triatomic FHH plane, D^{J}_{Mk} is a Wigner rotation matrix element,[28] $g^{Jk}_{vj}(R)$ describes the stretch of the HF–H complex, and the coordinate representation of the $\left|\mathrm{v}jk\right\rangle$ ket is

$$\left\langle r\gamma \middle| \mathrm{v}jk \right\rangle = Y_{jk}(\gamma,0) \frac{\phi_{\mathrm{v}j}(r)}{r} \ . \tag{5.11}$$

In this last equation $\phi_{\mathrm{v}j}(r)$ designates a complete set of functions which span the vibrational motion of the diatomic moiety and $Y_{jk}(\gamma,0)$ is a spherical harmonic.[28]

After premultiplication by $D^{J}_{M\mathcal{k}'}(\phi,\theta,\psi)Y_{j'k'}(\gamma,0)\phi_{\mathrm{v}'j'}(r)$ and integration over the variables ϕ_R, θ_R, ψ, γ, and r, the Schrödinger equation reduces to a set of coupled 2nd order differential equations in the functions $g^{Jk}_{vj}(R)$.

$$\left[-\frac{\hbar^2}{2\mu_{\mathrm{H,HF}}}\frac{d^2}{dR^2}+\frac{J(J+1)+j(j+1)-2k^2}{2\mu R^2}+\varepsilon_{\mathrm{v}j}+\langle \mathrm{v}jk|V(R,r,\gamma)|\mathrm{v}jk\rangle-E\right]g^{Jk}_{\mathrm{v}j}(R)$$
$$=-\sum_{\mathrm{v}'j'}\langle \mathrm{v}'j'k|V(R,r,\gamma)|\mathrm{v}jk\rangle g^{Jk}_{\mathrm{v}'j'}(R)+\sum_{k'}\langle \mathrm{v}jk'|\frac{\hat{l}^2}{2\mu R^2}|\mathrm{v}jk\rangle g^{Jk'}_{\mathrm{v}j}(R)\,. \tag{5.12}$$

The matrix elements of the centrifugal potential on the right-hand-side are[51-53]

$$\langle \mathrm{v}jk'|\frac{\hat{l}^2}{2\mu R^2}|\mathrm{v}jk\rangle=-\delta_{k',k\pm1}\left[J(J+1)-k(k\pm1)\right]^{1/2}\left[j(j+1)-k(k\pm1)\right]^{1/2} \tag{5.13}$$

We note that the matrix of the potential $V(R,r,\gamma)$ is diagonal in the projection quantum number k, while the matrix of the centrifugal potential is diagonal in v and j, but a banded tri-diagonal matrix in k.

Within the adiabatic-bender approximation, rather than solving this set of coupled equations, one first diagonalizes the matrix of the potential in the $|\mathrm{v}jk\rangle$ basis, with the addition of the diagonal $\varepsilon_{\mathrm{v}j}$ terms as a function of the separation coordinate R. Let us designate this matrix as $\mathbf{V}^{(Jk)}(R)$, so that

$$V^{(Jk)}_{\mathrm{v}j,\mathrm{v}'j'}(R)\equiv\left[\frac{J(J+1)+j(j+1)-2k^2}{2\mu R^2}+\varepsilon_{\mathrm{v}j}\right]\delta_{\mathrm{v}j,\mathrm{v}'j'}+\langle \mathrm{v}'j'k|V(R,r,\gamma)|\mathrm{v}jk\rangle\,. \tag{5.14}$$

Let us further denote the eigenvalues of $\mathbf{V}^{(Jk)}(R)$ as $\varepsilon^{(Jk)}_n(R)$, where n indexes the eigenvalues. These are called the adiabatic-bender potentials. The corresponding eigenvectors are designated $\mathbf{c}^{(Jk)}_n(R)$.

To obtain an estimate of the bound-state energies, one solves the one-dimensional Schrödinger equation for these adiabatic bender potentials

$$\left[-\frac{\hbar^2}{2\mu_{\mathrm{H,HF}}}\frac{d^2}{dR^2}+\varepsilon_n^{(Jk)}(R)-E_{ns}^{(Jk)}\right]g_{ns}^{(Jk)}(R)=0 \ . \tag{5.15}$$

The elements of the potential coupling matrix can be evaluated by expanding the H–HF triatomic potential $V(R,r,\gamma)$ in Legendre polynomials,

$$V(R,r,\gamma)=\sum_{\lambda}V_\lambda(R,r)P_\lambda(\cos\gamma) \ , \tag{5.16}$$

where

$$V_\lambda(R,r)=\frac{2\lambda+1}{2}\int_0^\pi V(R,r,\gamma)P_\lambda(\cos\gamma)\sin\gamma d\gamma \ . \tag{5.17}$$

Since the angular dependence of the $|\mathrm{v}jk\rangle$ functions is given by $Y_{jk}(\gamma,0)$ [Eq. (5.11)], the matrix elements of the potential in Eqs. (5.12) and (5.14) – the $\langle \mathrm{v}'j'k|V(R,r,\gamma)|\mathrm{v}jk\rangle$ matrix elements – can be simplified to give[21,52]

$$\begin{aligned}&\langle \mathrm{v}'j'k|V(R,r,\gamma)|\mathrm{v}jk\rangle \\ &=\sum_{\lambda=0}^{\infty}(-1)^k\left[(2j'+1)(2j+1)\right]^{1/2}\begin{pmatrix} j' & \lambda & j \\ 0 & 0 & 0\end{pmatrix}\begin{pmatrix} j' & \lambda & j \\ -k & 0 & k\end{pmatrix}\int\phi_{v'j'}(r)V_\lambda(R,r)\phi_{vj}(r)dr \ ,\end{aligned} \tag{5.18}$$

where (:::) is a Wigner 3*j* coefficient.[28] Note that the matrix elements of *V* are independent of the total angular momentum *J*.

For HF–H, the minima in the adiabatic bender potentials all lie at $R\cong 6$ bohr. For *R* greater than ~ 5 bohr, the potential is nearly vibrationally adiabatic, so that

$$\int\phi_{\mathrm{v}'j'}(r)V_\lambda(R,r)\phi_{\mathrm{v}j}(r)dr\cong 0 \tag{5.19}$$

for v'≠v. Thus, for simplification, we eliminated all states with v≠3 in Eq. (5.9). The one-dimensional adiabatic bender equations were then solved numerically. As a further simplification we invoked the coupled-states approximation,[51,54] wherein all Coriolis coupling between states with different k is neglected, so that the dimension of the $\mathbf{V}^{(Jk)}(R)$ matrix is equal to the number of rotational levels included in the expansion in Eq. (5.9).

5.4 Results

Figure 5.5 displays the k=0 adiabatic bender curves, $\varepsilon_n^{(J,k=0)}(R)$, that correlate asymptotically with HF(v=3, j=0,1,2,3,4)+H. The lowest curve (n=1) correlates with HF(v=3, j=0) +H, the next curve (n=2) correlates with HF(v=3, j=1)+H, etc. All the curves have a minimum at $R \cong 6$ bohr. This corresponds to the shallow van der Waals well in the H–HF valley of the SW-PES. The corresponding bound-state eigenvalues $E_{ns}^{(J,k=0)}$ were calculated by solving numerically Eq. (5.15). Here, the index s (s=0, 1, 2, …) indicates the degree of excitation of the van der Waals stretch mode in the n^{th} adiabatic bender curve associated with total angular momentum J and projection quantum number k. We used a fixed-stepsize DVR method, similar to that proposed by Colbert and Miller.[55] A total of 20 rotational functions (j=0–19) was necessary to obtain fully converged adiabatic-bender potentials.

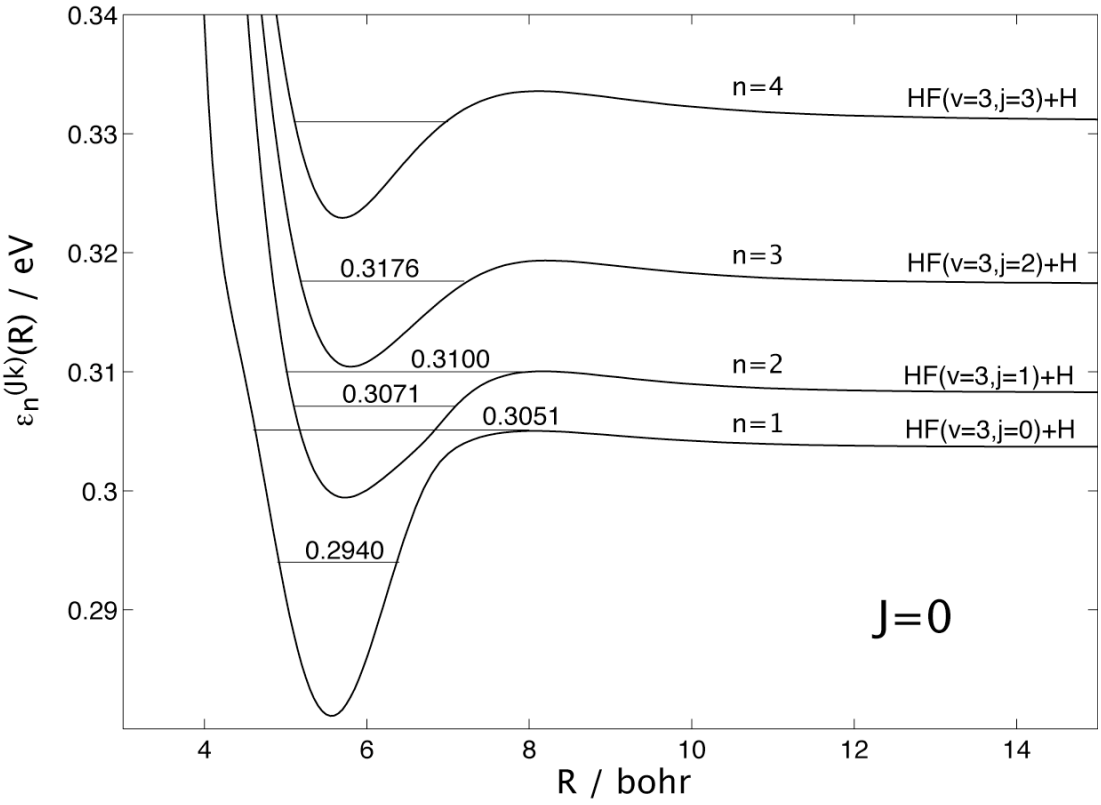

Figure 5.5 The first five adiabatic bender potentials for J=0 and k=0. The positions of the calculated quasi-bound states are shown.

We observe that for J=0 each of the lower adiabatic bender curves supports at least one bound state, whose position is indicated in Fig. 5.5. Note that when we include the coupling between the individual adiabatic bender states, and the coupling between adiabatic states with v=0, 1, and 2, the bound states which are shown schematically in Fig. 5.4 become only quasi-bound. When the collision energy of the HF(v=3, j=0)+H collision energy equals the energies of these quasi-bound states, then interference will occur between the scattering wavefunction and the wavefunction corresponding to this quasi-bound state. This will give rise to a resonance, with the

appearance of rapid variations in the energy dependence of the integral cross sections. In a time-dependent picture, these resonances will give rise to splitting, and delaying, of the initial scattering wavepacket.[39,45]

Comparison of the energies of these J=0 adiabatic-bender bound states with the energy dependence of the J=0 partial removal probability (Fig. 5.3), reveals that each of the subtle features seen in Fig. 5.3 and 5.4 occurs at an energy which is within a few meV of the position of an adiabatic bender level. In particular, the prominent peak at E=0.3052 eV in the J=0 partial removal probability corresponds to the n=1, s=1 quasi-bound state. We note, however, that the lowest bend-stretch state (n=1, s=0, E=0.2940) lies below the HF(v=3, j=0)+H asymptote [E =0.3035 eV, relative to F+H_2(r=r_e)], and thus will not be accessible in the scattering.

As the total angular momentum increases, the increasing centrifugal term in Eq. (9) will raise the adiabatic-bender potentials, in what is commonly referred to as "J shifting."[19] This is illustrated in Fig. 5.6, which displays the lowest (n=1) adiabatic bender potentials for k = 0 and J = 0, 5, 9, 10, and 11. Consequently, the energies of the quasi-bound states $E_{ns}^{(Jk)}$ will increase with J. This can be seen in Tables 5.1 and 5.2, which list the energies of the n=1, s=0 and n=1, s=1 states as a function of J.

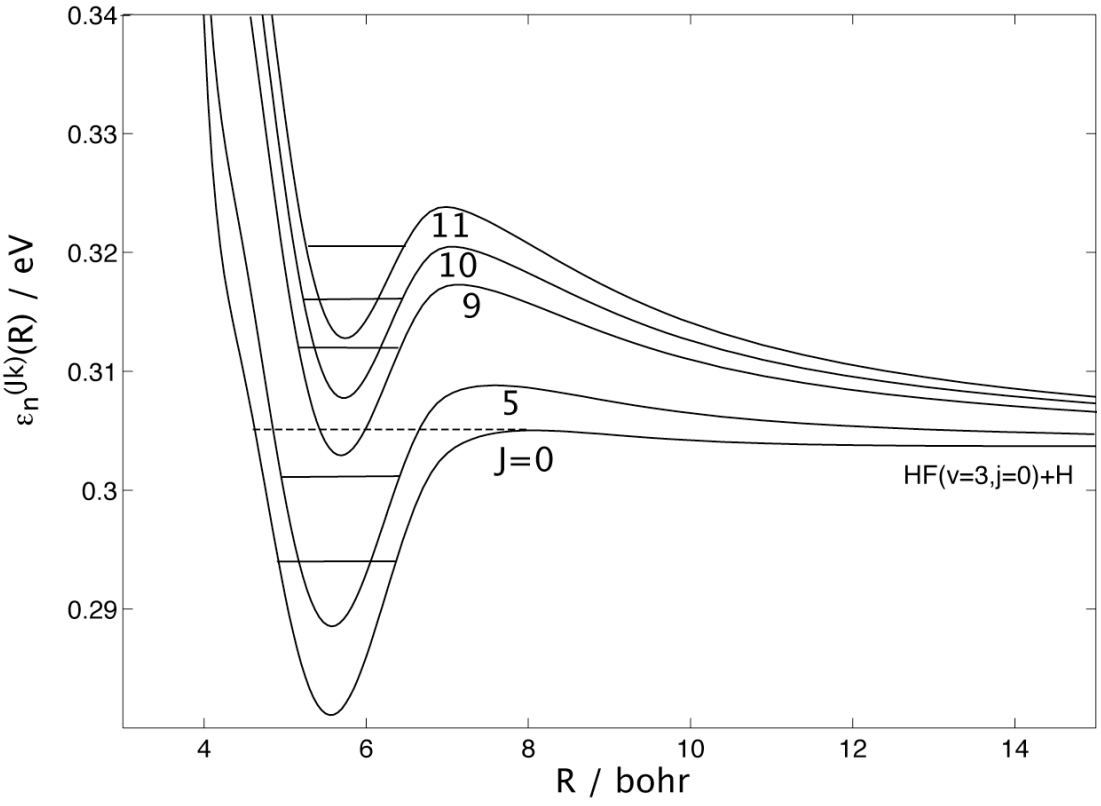

Figure 5.6 The lowest adiabatic bender (n=1) potential for k=0 and J = 0, 5, 9, 10, and 11. The positions of the s=0 quasi-bound levels are shown by solid horizontal lines. The dashed horizontal line indicates the position of the next higher (s=1) level for J=0.

Table 5.1 Energies of the v=3, k=0, n=1, s = 0 quasi-bound HF–H van der Waals states on the SW-PES. [a]

J	$E_{ns}^{(J,k=0)}$
0	0.2940
2	0.2966
5	0.3012
7	0.3031
8	0.3086
9	0.3122
10	0.3162
11	0.3208
12	0.3257
13	0.3302
14	… [b]

a. Energies in eV, relative to F+H_2(r=r_e).

b. For $J \geq 14$ no bound states exist for the v=3, k=0, n=1 adiabatic-bender potentials.

Table 5.2 Energies of the v=3, k=0, n=1, s = 1 quasi-bound HF–H van der Waals states on the SW-PES. [a]

J	$E_{ns}^{(J,k=0)}$
0	0.3051
2	0.3058
5	0.3088
7	0.3125
8	… [b]

a. Energies in eV, relative to F+H_2(r=r_e).

b. For $J \geq 8$ no s=1 bound states exist for the v=3, k=0, n=1 adiabatic-bender potentials.

We see that the first peak in the partial removal probabilities for J = 0, 2, 5, and 8 shown in Fig. 5.3 also shifts to higher energy with increasing J, and, in every case the position of this peak corresponds extremely closely to the energies of the n=1, s=1 quasi-bound states listed in Table 5.1. If the increase in the position of the bound states were a consequence of J-shifting, then the energies would scale as $J(J+1)$. Fitting the energies tabulated in Tables 5.1 and 5.2 to the formula

$$E_{ns}^{(Jk)} = E_{ns}^{(0k)} + B_{ns}^{(k)} J(J+1) \quad , \tag{5.21}$$

gives, a value of $B_{10}^{(0)} = 0.187$ meV (1.50 cm^{-1}), with a rms error in the fit of 4 meV. For the s=1 states, the fit gives $B_{11}^{(0)} = 0.113$ meV (0.91 cm^{-1}), with a rms error in the fit of 1 meV. The s=1 states have a smaller rotational constant, because they are located at a larger HF–H distance.

As J increases, the n=0 adiabatic bender curves become too shallow to support more than one bound state. Consequently, the prominent peak in the partial removal probabilities which is associated with the s=1 resonance disappears, at J=8. However, as seen in Table 5.1, as J increases above 8, the position of the lowest adiabatic-bender quasi-bound state (n=1, s = 0), increases above the energy of the HF(v=3, j=0)+H asymptote (E=0.3035 eV). Consequently, for total angular momenta in the range $9 \leq J \leq 12$, additional resonances will occur, corresponding to these s=0 quasi-bound states. This is apparent in Fig. 5.4, which plots the partial removal rates out of HF(v=3, j =0) for J = 8–13. For values of the total angular momentum J >13, the adiabatic-bender curves are too shallow to support even a single bound state, so the resonances disappear.

The sharp structure due to the resonances survives the summation over J [Eq. (5.4)], so that the energy dependence of the integral removal cross sections shown in Fig. 5.1 reveals evidence of the low-J, s=1 quasi-bound states, manifest in the broad peak at low energy, and the high-J, s=0 quasi-bound states, manifest in the sharp peaks at higher energy.

More insight is gained by examining the probability density of the quasi-bound states, $\Phi^{Jk}(R,r,\gamma)^2$. Within the adiabatic-bender model, and, in particular, within the restriction that the expansion of the r dependence of $\Phi^{Jk}(R,r,\gamma)$ is limited, in Eqs. (5.9) and (5.12) to just the HF v=3 vibrational functions, we have (if we further restrict k to 0)

$$\Phi^{J,k=0}(R,r,\gamma) \cong g_{ns}^{(k=0)}(R)\sum_j \mathbf{c}_n^{(Jk=0)}(R)Y_{jk}(\gamma,0)\frac{\phi_{\mathrm{v}=3,j}(r)}{r} \quad . \tag{5.21}$$

Figures 5.7 and 5.8 show contour plots of the R,r dependence of $\Phi^{J,k=0}(R,r,\gamma)^2$ for the n=1, s=0 and 1 states for J=0 for HFH collinear geometry (γ=0), and superimposes these plots on plots of the SW potential energy surface. As we might have anticipated, since the r-dependence of $\Phi^{J,k=0}(R,r,\gamma)$ is restricted to just the HF v=3 vibrational functions, the r-dependence of the quasi-bound states displays the expected three-node topology of a v=3 vibrational functions. The R dependence is localized, again as we might have anticipated, in the region of the well in the adiabatic-bender curves. We also observe in Figs. 5.7 and 5.8, that for the values of R at which wavefunctions of the s=0 and, especially, the s=1 quasi-bound states are large, the r-dependence of the HF–H potential energy surfaces is little

different from what is seen asymptotically. This is an additional justification of the assumption of vibrational adiabaticity in our adiabatic-bender calculations.

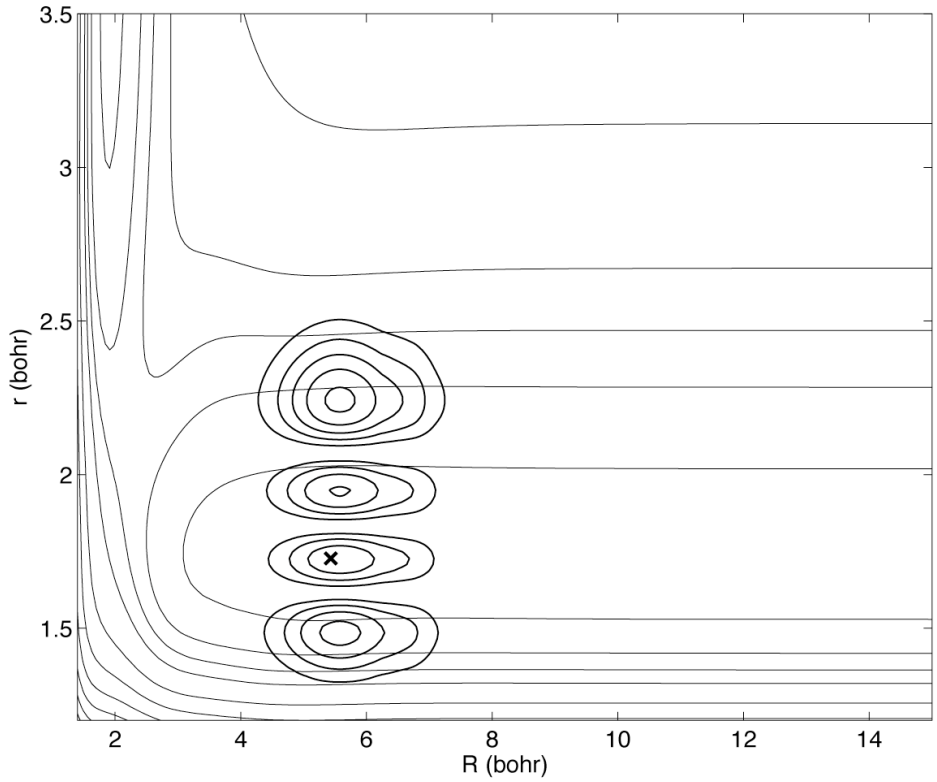

Figure 5.7 Contour plot of the square of the bend-stretch wavefunction $\Phi^{J,k=0}(R,r,\gamma)$ for the J=0, n=1, s=0 quasi-bound state, for collinear HFH geometry, superimposed on a contour plot of the Stark-Werner potential energy surface. The "X" marks the position of the van der Waals minimum. This plot clear shows a state with three nodes along the asymmetric stretch (r direction) and zero node in the symmetric stretch (R direction), thus assigned to (v=3, n=1, s=0) states

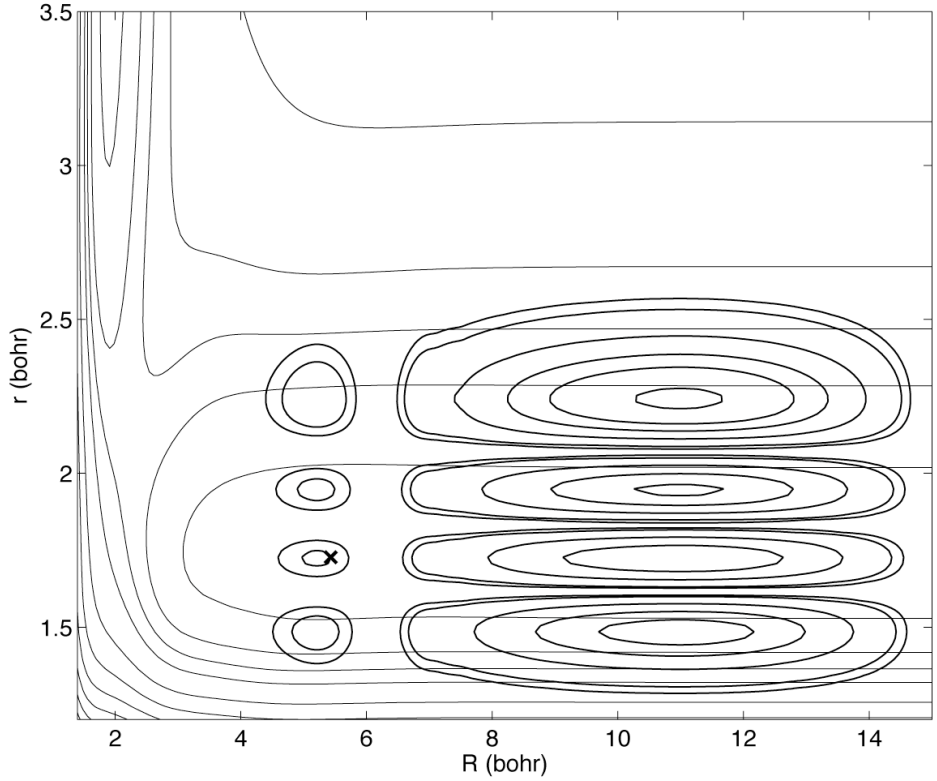

Figure 5.8 Contour plot of the square of the bend-stretch wavefunction $\Phi^{J,k=0}(R,r,\gamma)$ for the J=0, n=1, s=1 quasi-bound state, for collinear HFH geometry, superimposed on a contour plot of the Stark-Werner potential energy surface. The "X" marks the position of the van der Waals minimum. This plot clearly shows a state with three nodes along the asymmetric stretch (r direction) and one node in the symmetric stretch (R direction), thus assigned to (v=3, n=1, s=1) states

Figure 5.9 displays contour plots of the R,γ dependence of $\Phi^{Jk}(R,r,\gamma)^2$ for the n=1, s=0 states for J=0 and for r held at the equilibrium value in HF (r_e=1.73 bohr), and superimposes these plots on a contour plot of the SW potential energy surface. We see here that the quasi-bound HF–H states are located primarily at collinear HFH geometry, where the deepest van der Waals minimum occurs.

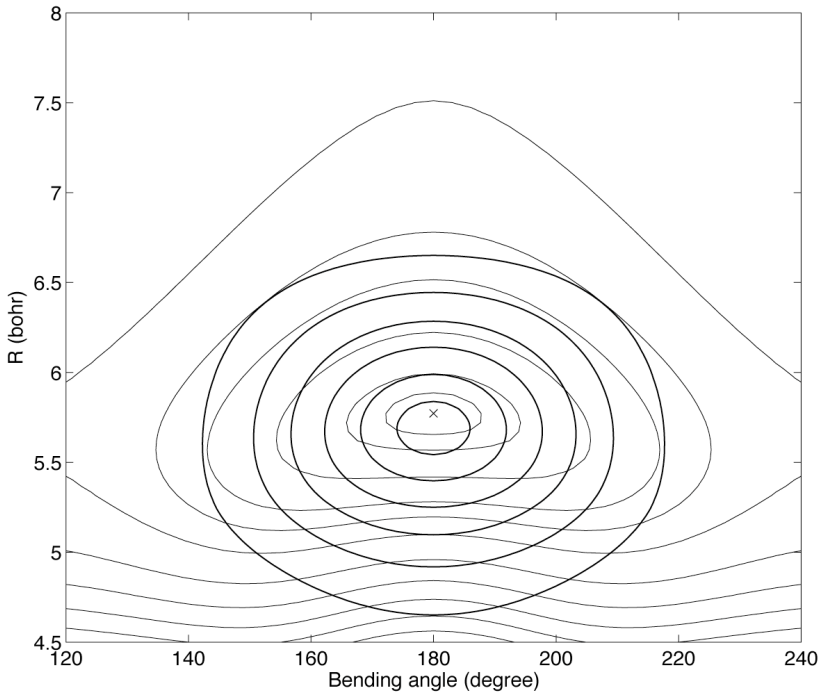

Figure 5.9 Contour plot of the square of the bend-stretch wavefunction $\Phi^{J,k=0}(R,r,\gamma)$ for the J=0, n=1, s=0 quasi-bound state, for an HF distance of r=r_e superimposed on a contour plot of the Stark-Werner potential energy surface. The "X" marks the position of the van der Waals minimum.

5.5 Rotational distributions

We see clearly in Fig. 5.1 that the presence of resonances leads to sharp enhancements in the vibrational removal cross sections. In principle, it might be possible for the final HF rotational distributions to be considerably altered by the presence of a long-lived resonance. To investigate this question we plot in Fig. 5.10 the dependence of the HF(v=3→2, 1) vibrationally inelastic cross sections at two energies, one corresponding to the narrow resonance peak at E_{tot} =0.3164 (Fig. 5.1) and the second (E_c=0.0155 eV) corresponding to the dip between the peaks at E_{tot} =0.3164 and E_{tot} = 0.3120 in Fig. 5.1.

In both cases, the rotational distributions correspond very closely to those we have already presented in Fig. 4.4. There appears very little difference between these distributions at a resonant collision energy and one off-resonance. Thus, we conclude that in the case of HF(v=3)+H vibrational relaxation, the presence of quasi-bound van der Waals states has little effect of the rotational distribution of the quenched HF molecules.

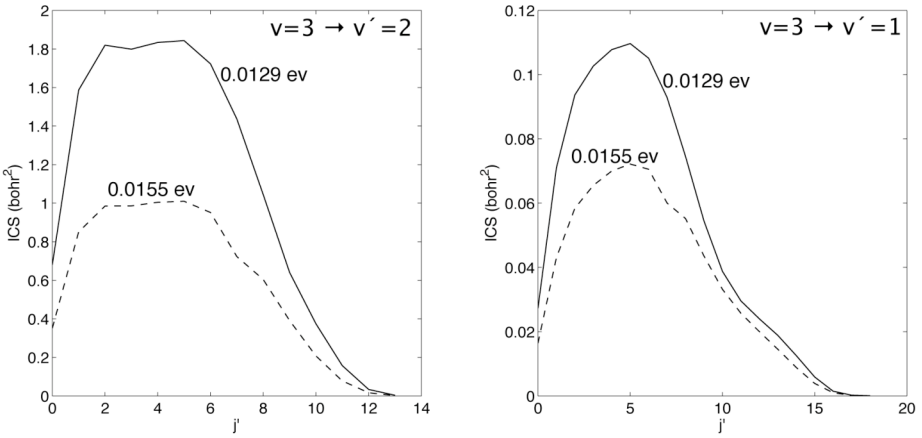

Figure 5.10 Integral cross sections into specific rotational states at two collision energies, the first (E_c=0.0129 eV) corresponding to the peak at E_{tot} =0.3164 (Fig. 5.1) and the second (E_c=0.0155 eV) corresponding to the dip between the peaks at E_{tot} =0.3164 and E_{tot} = 0.3120 in Fig. 5.1.

5.5 Discussion and conclusions

We have presented here a detailed study of the role of resonances in the vibrational relaxation of HF(v=3) by collisions with H atoms. Fully quantum reactive scattering calculations were presented of the overall removal cross section for HF(v=3) in collisions with H atoms. This involves three processes: vibrationally inelastic scattering with and without H-atom exchange, and reaction. Of these processes inelastic scattering without atom exchange is the dominant relaxation mechanism, followed by reaction. Inelastic scattering with atom exchange is least

probable, because at low collision energy this can occur only by quantum tunneling through the H···F···H exchange barrier.

The energy dependence of the removal cross section for each of these processes displays several narrow peaks. We have used an adiabatic-bender analysis, similar to that invoked by Castillo *et al.*[19] in an earlier study of reactive $F+H_2$ scattering, to analyze this structure. We have shown that the most prominent peaks correspond to shape resonances involving quasi-bound HF–H states which are trapped behind a combination of the HF–H centrifugal potential and the HF–H weak van der Waals attraction.

From a time-dependent point of view, trapping of the initial wavepacket in these quasi-bound states will increase the time the collision system is exposed to the weak coupling between v=3 and the lower vibrational manifolds, thus increasing the overall relaxation cross section. Because the peaks seen in the energy dependence of the total removal cross section are due to interactions between the scattering wavefunction and quasi-bound states in the HF–H valley, the coupling will effect all collisions, regardless of the final outcome (inelastic scattering with or without H atom exchange and reaction). Hence, as we see in Fig. 5.1, the resonance peaks are present in the removal cross sections for each of these processes.

Several recent *ab initio* studies of the HF–H region of the FHH potential energy surface have shown[50,56] that an artifact of the fit used by Stark and Werner will generate an small artificial barrier at large HF–H separations, outside of the van der Waals well. This barrier can be seen clearly in Fig. 5.5. This presence of this barrier might artificially enhance the importance of the n=1, s=1 quasi-bound states,

which, as can be seen in Figs. 5.5 and 5.6, are barely bound and might disappear if a more accurate fit were done which resulted in removal of this barrier. Alternatively, however, an improved *ab initio* treatment with a better description of the correlation energy could lead to a lowering in the HF–H van der Waals well, which would result in the s=1 states being bound regardless.

As we have discussed, it is only the lowest energy peak in the removal cross sections which is a reflection of the s=1 quasi-bound states. The peaks at higher energy are a reflection of coupling with the s=0 quasi-bound states. As we see in Figs. 5.5 and 5.6, these quasi-bound states are rather deeply bound in each adiabatic bender potential, and will certainly persist even in the absence of an artificial barrier at long range.

The present study focused exclusively on the relaxation of HF(v=3, j=0). It is likely that similar resonance effects, involving quasi-bound HF–H states, would play a role in the relaxation of other vibrational levels. As we have seen, the major resonance effects were rotationally adiabatic, in the sense that the quasi-bound states in the adiabatic bender potentials which correlated with HF(v=3, j=0)+H played the major role. We would expect then that for the relaxation of HF in rotational levels with $j\neq0$, it would be quasi-bound states in the higher ($n>1$) adiabatic bender potentials which would provide the major resonant coupling. As we see in Fig. 5.5, these higher ($j>0$) adiabatic bender potentials also support quasi-bound states.

Another extension of the present study would be to carry out a quantum time-dependent study of the HF+H vibrational removal dynamics, with a focus on the degree of time delay introduced by the resonant coupling with the quasi-bound states.

In addition, we certainly encourage the experimental study of the resonance effects uncovered here.

Chapter 6: Summary

In this dissertation we presented the results of a fully quantum mechanical investigation of the vibrational relaxation of HF(v) in collisions with H atoms. The comparison between earlier quasi-classical trajectory (QCT) calculations and fluorescence experiments motivated our investigation to provide more detailed and accurate predictions of the dynamics of H+HF inelastic scattering.

As outlined in Chapter 1, 30 years after the first experimental investigation of the relaxation of HF by H atoms, a key process in the HF chemical laser system, there is not yet satisfactory agreement between theoretical simulations and experiment. Likely this is due to inaccuracies in the approximate potential energy surface used in this early work, as well a purely classical treatment of the reaction dynamics, which does not allow quantum tunneling through the H–F–H reaction barrier. As outlined in Chapter 2, our investigation is based on the recently developed Stark-Werner *ab initio* potential energy surface (SW-PES). As we saw in the following chapters, the location and magnitudes of the saddle points and small wells on the SW-PES play significant roles in the reaction dynamics, in particular in defining the quasi-bound states which lead to resonant enhancement of the vibrational removal cross sections.

Chapter 3 reviewed the quantum scattering (coupled-channel) formalism in both space and body-fixed frames. We described fully the connection between the S matrices, which are the output of these scattering calculations, and the cross sections and rate constants which are the experimental observables. In particular, the use of a parity- and symmetry- adapted basis enables us both to reduce the overall size of the

basis, and the computational expense, and to separate out inelastic relaxation with and without H atom exchange, which are not possible to distinguish experimentally.

In Chapter 4, our results show that deactivation of HF(v=3) is a very fast process with rate constants on the order of 10^{13} cm^3-mol/sec. Because of the high reaction barrier, atom exchange contributes little to the deactivation of HF(v=2). For the vibrational relaxation from highly excited vibrational states, such as HF(v=4,5), multiple quantum transitions contribute significantly to the overall removal cross section, while for HF(v≤3), vibrational relaxation occurs mainly through single quantum transitions. Quantum mechanical calculations also show that inelastic (HF+H) energy transfer is primarily a V→T process, involving vibrational energy conversion into translational energy, with V→R conversion of vibrational to rotational energy playing only a minor role. Overall, our quantum calculations based on an *ab initio* potential energy surface agree better with the limited experimental data than the earlier quasi-classical simulations.

Chapter 5 invokes an adiabatic bender model to explain successfully the prominent resonance peaks in the energy dependence of the cross sections for the relaxation of HF(v=3, *j*=0). These peaks correspond to shape resonances involving quasi-bound HF–H states which are trapped behind a combination of the HF–H centrifugal potential and the HF–H weak van der Waals attraction.

Again, all of our calculations and conclusions depend critically on the features of the SW potential energy surface (van der Waals wells and barrier heights). Since this work is the first quantum mechanical investigation on H+HF reactions, more work need to be done in the future. For example, one major task in the future is that

we need to calculate the exact vibrational relaxation rate constant for a wide range of temperature. The finer grid of energies is encouraged to be used for quantum tunneling, in order to map out more detailed resonance feathers. Since the experimental data are 30 years old, we encourage some scientists to re-measure the vibrational relaxation rate constants for each channel. The challenge here might be the difficulty in measuring the rate for each reaction directly.

The most surprising and interesting discovery in this thesis is the role of resonances in the vibrational relaxation of HF(v=3, j=0). As we can see in Fig. 5.5, the higher (j > 0) adiabatic bender potentials also support quasi-bound states, which indicates that we might expect to find resonance fingerprints in the relaxation of HF(v=3, j > 0). Also, it is likely that similar resonance effects, involving quasi-bound HF-H states, will play a role in the relaxation of other vibrational levels. Therefore, future theoretical studies might focus on the relaxation of these other rotational or vibrational levels, in the search for resonance fingerprints.

Additional time-dependent theoretical techniques, specifically wave-packet methods or the use of time-delay tools, would cast additional light on the nature of the van der Waals resonances we have uncovered. A broader theoretical endeavor would the search for the signature of similar weakly-bound states in other collision events. Alternatively we encourage future experimental study of the role of resonances in HF+H vibrational relaxation. Eventually, discovery of these resonances could provide valuable experimental input into a future refinement of the FH_2 potential energy surface.

Bibliography

[1] A. Benshaul, K. L. Kompa, and U. Schmailzl, J. Chem. Phys. **65**, 1711 (1976).

[2] M. J. Berry and G. C. Pimentel, J. Chem. Phys. **49**, 5190 (1968); N. G. Basov, *Chemical Lasers*. (Springer-Verlag, Berlin, Germany 1990).

[3] H. L. Chen, R. L. Taylor, J. Wilson, P. Lewis, and W. Fyfe, J. Chem. Phys. **61**, 306 (1974).

[4] G. C. Manke and G. D. Hager, J. Phys. Chem. Refer. Data **30**, 713 (2001).

[5] Y. T. Lee, Science **236**, 793 (1987).

[6] J. F. Bott and R. F. Heidner, J. Chem. Phys. **72**, 3211 (1980).

[7] D. L. Thompson, J. Chem. Phys. **57**, 4170 (1972).

[8] R. L. Wilkins, J. Chem. Phys. **58**, 3038 (1973).

[9] S. R. Leone, J. Phys. Chem. Refer. Data **11**, 953 (1982).

[10] S. A. Nizkorodov, W. W. Harper, and D. J. Nesbitt, Faraday Disc. Chem. Soc. **113**, 107 (1999).

[11] J. F. Bott and R. F. Heidner, J. Chem. Phys. **68**, 1708 (1978).

[12] J. F. Bott and R. F. Heidner, J. Chem. Phys. **66**, 2878 (1977).

[13] R. F. Heidner and J. F. Bott, J. Chem. Phys. **63**, 1810 (1975).

[14] D. L. Thompson, J. Chem. Phys. **56**, 3570 (1972); T. Takayanagi and S. Sato, Chem. Phys. Lett. **144**, 191 (1988).

[15] R. L. Wilkins, Mol. Phys. **29**, 555 (1975).

[16] K. Stark and H. J. Werner, J. Chem. Phys. **104**, 6515 (1996).

[17] P. J. Knowles, K. Stark, and H. J. Werner, Chem. Phys. Lett. **185**, 555 (1991).

[18] J. F. Castillo, B. Hartke, H. J. Werner, F. J. Aoiz, L. Banares, and B. Martinez-Haya, J. Chem. Phys. **109**, 7224 (1998).

[19] J. F. Castillo, D. E. Manolopoulos, K. Stark, and H. J. Werner, J. Chem. Phys. **104**, 6531 (1996).

[20] J. F. Castillo and D. E. Manolopoulos, Faraday Disc. Chem. Soc. 119 (1998).

[21] W. H. Miller, *Dynamics of molecular collisions*, Part A (Plenum, New York and London, 1976).

[22] R. T. Pack and G. A. Parker, J. Chem. Phys. **87**, 3888 (1987).

[23] G. C. Schatz and A. Kuppermann, J. Chem. Phys. **65**, 4642 (1976).

[24] D. Skouteris, J. F. Castillo, and D. E. Manolopoulos, Comput. Phys. Commun. **133**, 128 (2000).

[25] L. M. Delves, Nucl. Phys. **20**, 275 (1960); B. R. Johnson, J. Chem. Phys. **73**, 5051 (1980); B. R. Johnson, J. Chem. Phys. **79**, 1916 (1983).

[26] R. T. Pack, J. Chem. Phys. **60**, 633 (1974).

[27] F. T. Smith, Physical Review **120**, 1058 (1960); F. T. Smith, J. Chem. Phys. **31**, 1352 (1959).

[28] D. M. Brink and G. R. Satchler, *Angular momentum*, 2nd ed. (Clarendon P., Oxford, 1968).

[29] R. N. Zare, *Angular Momentum* (Wiley, New York, 1988).

[30] I. W. M. Smith, *Kinetics and dynamics of elementary gas reactions* (Butterworths, London, 1980).

[31] R. D. Levine and R. B. Bernstein, *Molecular Reaction Dynamics and Chemical Reactivity* (Oxford University Press, New York 1987).

[32] R. N. Schwartz, Z. I. Slawsky, and K. F. Herzfeld, J. Chem. Phys. **20**, 1591 (1952); J. D. Lambert, *Vibrational and Rotational Relaxation in Gases*. (Clarendon, Oxford, U.K., 1977).

[33] W. H. Miller, J. Chem. Phys. **62**, 1899 (1975); W. H. Miller, Accounts Chem. Res. **26**, 174 (1993).

[34] S. Atahan, *PhD thesis*, University of Maryland, 2006; S. Atahan and M. H. Alexander, J. Phys. Chem. A **110**, 5436 (2006).

[35] E. J. Rackham, T. Gonzalez-Lezana, and D. E. Manolopoulos, J. Chem. Phys. **119**, 12895 (2003); E. J. Rackham, F. Huarte-Larranaga, and D. E. Manolopoulos, Chem. Phys. Lett. **343**, 356 (2001).

[36] R. V. Krems and S. Nordholm, J. Chem. Phys. **115**, 10581 (2001).

[37] S. E. Bradforth, D. W. Arnold, D. M. Neumark, and D. E. Manolopoulos, J. Chem. Phys. **99**, 6345 (1993); Y. T. Lee, Science **236**, 793; D. M. Neumark, A. M. Wodtke, G. N. Robinson, C. C. Hayden, and Y. T. Lee, J. Chem. Phys. **82**, 3045 (1985); M. H. Qiu, Z. F. Ren, L. Che, D. X. Dai, S. A. Harich, X. Y. Wang, X. M. Yang, C. X. Xu, D. Q. Xie, M. Gustafsson, R. T. Skodje, Z. G. Sun, and D. H. Zhang, Science **311**, 1440 (2006); G. C. Schatz, J. M. Bowman, and A. Kuppermann, J. Chem. Phys. **58**, 4023 (1973); D. E.

Manolopoulos, K. Stark, H. J. Werner, D. W. Arnold, S. E. Bradforth, and D. M. Neumark, Science **262**, 1852 (1993).

[38] S. D. Chao and R. T. Skodje, J. Chem. Phys. **113**, 3487 (2000).

[39] S. D. Chao and R. T. Skodje, J. Chem. Phys. **119**, 1462 (2003).

[40] T. Takayanagi and Y. Kurosaki, J. Chem. Phys. **109**, 8929 (1998).

[41] K. Liu, R. T. Skodje, and D. E. Manolopoulos, Phys. Chem. Comm., 27 (2002).

[42] R. N. Zare, Science **311**, 1383 (2006).

[43] B. K. Kendrick, L. Jayasinghe, S. Moser, M. Auzinsh, and N. Shafer-Ray, Phys. Rev. Lett. **84**, 4325 (2000); G. C. Schatz and A. Kuppermann, J. Chem. Phys. **59**, 964 (1973).

[44] R. T. Skodje, D. Skouteris, D. E. Manolopoulos, S. H. Lee, F. Dong, and K. Liu, J. Chem. Phys. **112**, 4536 (2000); R. T. Skodje, D. Skouteris, D. E. Manolopoulos, S. H. Lee, F. Dong, and K. P. Liu, Phys. Rev. Lett. **85**, 1206 (2000).

[45] C. L. Russell and D. E. Manolopoulos, Chem. Phys. Lett. **256**, 465 (1996).

[46] B. B. Grayce and R. T. Skodje, J. Chem. Phys. **95**, 7249 (1991).

[47] R. T. Skodje, J. Chem. Phys. **95**, 7234 (1991).

[48] S. L. Holmgren, M. Waldman, and W. Klemperer, J. Chem. Phys. **67**, 4414 (1977).

[49] M. H. Alexander, S. Gregurick, and P. J. Dagdigian, J. Chem. Phys. **101**, 2887 (1994).

[50] M. H. Alexander, F. Lique, G. Li, and H.-J. Werner, to be published.

[51] P. McGuire and D. J. Kouri, J. Chem. Phys. **60**, 2488 (1974).

[52] R. T. Pack, J. Chem. Phys. **60**, 633 (1974).

[53] M. H. Alexander, D. E. Manolopoulos, and H. J. Werner, J. Chem. Phys. **113**, 11084 (2000).

[54] D. J. Kouri, in *Atom-Molecule Collision Theory: A Guide for the Experimentalist*, edited by R. B. Bernstein (Plenum, New York, 1979), pp. 301.

[55] D. T. Colbert and W. H. Miller, J. Chem. Phys. **96**, 1982 (1992).

[56] M. Hayes, M. Gustafsson, A. M. Mebel, and R. T. Skodje, Chem. Phys. **308**, 259 (2004).